 CMES, vol.48, no.1, pp.43-82, 2009

On the Convergence of Random Differential Quadrature (RDQ) Method and Its Application in Solving Nonlinear Differential Equations in Mechanics

Hua Li[1], **Shantanu S. Mulay**[1] **and Simon See**[2]

Abstract: Differential Quadrature (DQ) is one of the efficient derivative approximation techniques but it requires a regular domain with all the points distributed only along straight lines. This severely restricts the DQ while solving the irregular domain problems discretized by the random field nodes. This limitation of the DQ method is overcome in a proposed novel strong-form meshless method, called the random differential quadrature (RDQ) method. The RDQ method extends the applicability of the DQ technique over the irregular or regular domains discretized using the random field nodes by approximating a function value with the fixed reproducing kernel particle method (fixed RKPM), and discretizing a governing differential equation by the locally applied DQ method. A superconvergence condition is developed for the RDQ method, which gives more than $O(h^{p+1})$ function value convergence for the uniform as well as random field nodes scattered in the domain. The RDQ method convergence analysis is carried out, and the superconvergence condition is verified by solving several 1D, 2D and elasticity problems. The applicability of the RDQ method to solve the nonlinear governing differential equations is successfully demonstrated by solving the fixed-fixed and cantilever beams for deflection due to the nonlinear electrostatic loading. It is concluded that the RDQ method effectively handles the irregular or regular domains discretized by the uniform or random field nodes, with good convergence rates.

Keywords: Meshless method, Fixed reproducing kernel particle method, Random differential quadrature method, Convergence analysis, Nonlinear beam equation, Elasticity problems.

[1] School of Mechanical and Aerospace Engineering, Nanyang Technological University, 50 Nanyang Avenue, Singapore 639798, Republic of Singapore

[2] Asia Pacific Science and Technology Center, Sun Microsystems, Inc., 1 Magazine Road, Singapore, 059567, Republic of Singapore

1 Introduction

Meshless methods are in a research area for the past 40 years but the extensive studies have been carried out in the last decade when people realized its potential to solve the large deformation and moving boundary problems. It can be broadly categorized into two types based on how the governing differential equation is solved: strong- (collocation based) and weak-forms (Galerkin approach based). Some of the earlier methods which were developed based on the weak-form approach include the smooth particle hydrodynamics (SPH) [Lucy (1977); Gingold and Monaghan (1977)], the diffuse element method [Nayroles, Touzot and Villon (1992)], the element-free Galerkin method [Belytschko, Gu and Lu (1994); Belytschko, Lu and Gu (1994); Lu, Belytschko and Gu (1994)], the natural element method [Braun and Sambridge (1995)], the reproducing kernel particle method (RKPM) [Liu, Jun and Zhang (1995); Liu, Chen, Uras and Chang (1996); Liu and Jun (1998)], the partition of unity [Melenk and Babuska (1996)], the meshless local Petrov-Galerkin approach (MLPG) [Atluri and Zhu (1998)], the local boundary integral equation method [Zhu, Zhang and Atluri (1998); Atluri, Sladek, Sladek and Zhu (2000)], the point interpolation method [Liu and Gu (2001)], and the local Kriging method [Li, Wang and Lam (2004)]. In most of these methods, the least square approximation or the reproducing kernel particle interpolation functions are combined with Galerkin or the variational weak form of the governing differential equation. Earlier methods developed based on the strong-form approach include the finite point method [Onate, Idelsohn, Zienkiewicz and Taylor (1996); Onate, Idelsohn, Zienkiewicz, Taylor and Sacco (1996)], Hermite cloud method [Li, Ng, Cheng and Lam (2003)], and the gradient smoothing method [Liu, Zhang, Lam, Li, Xu, Zhong, Li and Han (2008)]. All these methods were successfully applied to solve different types of engineering problems [Atluri, Cho and Kim (1999); Atluri, Kim and Cho (1999); Gilhooley, Xiao, Batra, McCarthy and Gillespie (2008); Idelsohn, Onate, Calvo and Pin (2003); Li, Wang and Lam (2004); Li, Yew, Ng and Lam (2005); Liu, Zhang, Li, Lam and Bernard Kee (2006); Onate, Idelsohn, Zienkiewicz, Taylor and Sacco (1996); Sukumar, Moran and Belytschko (1998); Sukumar, Moran, Semenov and Belicov (2001)]. The weak-form meshless methods are considered numerically more stable than those based on the strong form. But the strong form methods can well capture the local high gradients, easy to implement, and are cheap in the computation.

Most of the weak form methods require some kind of background mesh to carry out the weak form integration but the MLPG method is a truly meshless method, which is applied over a local domain, based on the local symmetric weak form. Atluri (2004), Atluri (2005), and Atluri and Shen (2002) discussed the MLPG method in detail with its application in the fluid and solid mechanics, respectively. Atluri

and Shen (2002) discussed different global and local trial and test functions and provided a broad framework under which different MLPG forms can be derived by combining it with the different local trial and test functions. Several MLPG mixed schemes are proposed like, finite difference method through MLPG [Atluri, Liu and Han (2006b)], finite volume method through MLPG [Atluri, Han and Rajendran (2004)], MLPG mixed collocation method [Atluri, Liu and Han (2006a)]. These MLPG mixed schemes and the MLPG method are applied to solve various engineering analysis problems like large deformation [Han, Rajendran and Atluri (2005)], 3D contact problems [Han, Liu, Rajendran and Atluri (2006)], heat conduction [XueHong, Shen and Tao (2007)], crack analysis in the 2D and 3D domains [Sladek, Sladek, Zhang, Solek and Starek (2007)], thermo-piezoelectricity [Sladek, Sladek, Zhang and Solek (2007)], and shell deformation [Jarak, Soric and Hoster (2007)]. Cai and Zhu (2008) modified the original MLPG method to overcome Shepard partition of unity (PU) approximation drawbacks by employing a new PU based Shepard and least square interpolation approximation. Liu, Chan, Li and Cen (2008) developed a method for the structural dynamic problems, constructing the trial functions by the natural neighbour concept and using them with the general MLPG method. Several researchers modified the MLPG method to solve the specific engineering problems like, solving Navier-Stokes and energy equations [Arefmanesh, Najafi and Abdi (2008)], limit analysis of plastic collapse [Chen, Liu and Cen (2008)], microelectromechanical systems [Dang and Sankar(2008)], topology optimization [Li and Atluri (2008); Zheng, Long, Xiong and Li (2009)], elastoplastic fracture analysis [Long, Liu and Li (2008)], steady state and transient heat conduction analysis in the 3D solid [Sladek, Sladek, Tan and Atluri (2008)], boundary and initial value problems in piezo-electric and magneto-electric-elastic solids [Sladek, Sladek, Solek and Atluri (2008)], thermal bending of Reissner-Mindlin plates [Sladek, Sladek, Solek and Wen (2008)], and 3D potential problems [Pini, Mazzia and Sartoretto (2008)].

The radial basis function (RBF) based collocation method was used to solve the modified equal width wave equation [Haq, Siraj and Ali (2008)], the Sturm-Liouville problem [Reutskiy (2008)], coupled heat transfer and fluid flow problem in Darcy porous media [Kosec and Šarler (2008)], the nonlinear Schrodinger Equations [Haq, Siraj and Uddin (2009)], and modeling of dynamic strain localization in quasi-brittle materials [Le, Mai-Duy, Tran-Cong and Baker (2008)]. Mai-Cao and Tran-Cong (2008) proposed a new meshless method, based on the level set method and semi-Lagrangian method coupled with the indirect RBF network method (IRBFNM), to capture the moving interfaces in passive transport problems; they also applied the IRBFNM to solve transient problems by combining it with different time integration schemes [Mai-Cao and Tran-Cong (2005)]. Young, Chen and Lee (2005)

developed a method based on potential theory and desingularization technique and applied it to acoustic problems [Young, Chen and Lee (2006)].

It was observed that the originally proposed SPH method [Lucy (1977)] is not able to reproduce the higher order terms well and is not able to satisfy the consistency condition when solving the problems with finite boundaries. Hence, it was enhanced over the last decade to improve its consistency and the stability aspects [Bonet, Lok (1998); Liu, Jun and Zhang (1995); Liu, Chen, Uras and Chang (1996); Liu and Jun (1998)]. Liu, Jun and Zhang (1995), and Liu, Chen, Uras and Chang (1996), and Liu and Jun (1998) modified the SPH window function by introducing a correction function term and called it as the RKPM; the new SPH window function is called the modified window function. As the RKPM is inherited from the SPH method, it has also inherited the SPH characteristics such as the smoothening of a function value over a local domain by an integral approximation. Because of the ability of higher order reproducibility, the RKPM is more widely used now than the original SPH method. Wong and Shie (2008) carried out the large deformation analysis by the SPH based Galerkin method with the moving least square (MLS) approximation; Wu, Chiu and Wang (2008) proposed a differential RKPM, in which separate differential reproducing condition sets were developed to compute the derivative shape functions instead of conventionally computing them by directly taking the RKPM approximation derivative. Aluru (2000) combined the RKPM interpolation function with the point collocation method to form a novel strong-form method. Aluru (1999), Aluru and Li (2001), Li, Paulino and Aluru (2003), Jin, Li and Aluru (2004), and Jin, Li and Aluru (2005) also presented different variations of the RKPM viz. fixed, moving and multiple fixed kernels, and combined the fixed RKPM with the point collocation method and called it the finite cloud method [Aluru and Li (2001)]. Li, Liu and Wang (2008) used the RKPM method to carry out the ductile fracture simulations and shown that they are in well agreement with the finite element method (FEM) and the existing experimental data.

Following the idea of an integral Quadrature, Bellman, Kashef and Casti (1972) proposed the DQ method. As per it, the derivative at any point is approximated by the weighted sum of function values in whole domain provided that all the points are collinear. It means that the important task in the DQ method is to determine the weighting coefficients. Bellman, Kashef and Casti (1972) suggested two approaches to compute the weighting coefficients. The first approach is the use of polynomial function as a test function, and the second one uses the test function, in which the co-ordinates of the grid points are chosen as the roots of the shifted Legendre polynomials. Both of these approaches have a problem when the order of algebraic system of equations is very large, making the resulting matrix highly ill-

conditioned. To overcome this problem, Quan and Chang (1989a), and Quan and Chang (1989b) proposed another approach, in which the weighting coefficients are computed using Lagrange interpolation polynomials. Shu, Khoo and Yeo (1994) proposed a general approach, in which they combined both Bellman, and Quan and Chang approaches. Using the linear vector space analysis, Shu (2000) proved that the polynomials used in Bellman, and Quan and Chang approaches are nothing but the different sets of base polynomial vectors of function approximation. If one of the base vectors satisfies the function approximation equation so will the other base vectors, which means that all the approaches will lead to the same values of the weighting coefficients and in turn similar function approximations. Shan, Shu and Lu (2008) coupled the local multiquadric-based RBF with the DQ method to solve the 3D curved boundary fluid flow problems. Liew, Zhang, Ng and Meguid (2003) applied the DQ method to model the elastic bonding in the 3D composite laminates. Liew, Huang and Reddy (2003) applied the MLS based DQ (MLSDQ) to solve the moderately thick plate for the shear deformation; they also applied the MLSDQ method to solve the 4^{th}-order thin plate bending differential equation over the irregular boundaries [Liew, Huang and Reddy (2004)]. More work about the DQ method can be found in Shu (2000), and Naadimuthu, Bellman and Wang (1984), and Ding, Shu, Yeo and Xu (2006).

The DQ method is an efficient numerical derivative approximation technique but one of its key requirements is to have a collinear field node arrangement hence, it is restricted to solve the problems involving the field nodes distributed only in a fixed pattern over the uniform domains. The main objective of the presented work is to overcome this limitation of the DQ method through the development of RDQ method, and carry out its thorough convergence analysis. During the convergence analysis studies, the superconvergence condition is developed, which always gives function value convergence greater than $O(h^{p+1})$, where p is the complete function approximation monomial order used. For the test problems solved in the presented work by the superconvergence condition, the convergence rates of $O(h^{p+\alpha})$, where $\alpha \geq 1$ for function approximation and $\alpha \approx 0.7$ to 1 for its derivative approximation, are obtained for uniform as well as the randomly distributed field nodes. Further, the RDQ method is applied to study the fixed-fixed and cantilever beams for deflection under the application of nonlinear electrostatic loading.

The motivation behind the development of the RDQ method is to extend the applicability of the DQ method over an irregular domain discretized by random or uniform field nodes, or a regular domain discretized by the random field nodes. Therefore, by given set of nodes (in arbitrary or fixed pattern) distributed over a domain (uniform or non-uniform), the RDQ method solves the governing partial differential equation (PDE) along with the appropriate boundary conditions (BC)

in its strong form. This is achieved by creating the background or auxiliary set of nodes, called the virtual nodes, over the computational domain as shown in Fig. 1. The function values at these virtual nodes are approximated in terms of the nodal parameter values of the surrounding field nodes by the fixed RKPM interpolation. Thus, a linear transformation matrix in the form of shape function values is associated with the nodal parameter values at the field nodes with the approximate function values at the virtual nodes. The derivative terms from the governing PDE are discretized at the virtual nodes by the locally applied DQ method. By means of the earlier developed transformation matrix, the derivative approximation equations at the virtual nodes are expressed in the form of unknown field node parameter values. All the BCs are imposed in the strong form. The PDE discretization equations are combined with the BC equations to give a global system of equations, which can be solved by any solver. In order to avoid the DQ method getting unstable as demonstrated by Zong and Lam (2002), it is applied locally, i.e. a local DQ domain is created around each virtual node in the x and y directions, the virtual nodes falling in it are taken into consideration for the derivative approximation at the central virtual node.

Compared with the existing strong-form meshless methods, the merit of the RDQ method is that the fixed RKPM function is used only to approximate the function values at virtual nodes and not to approximate the derivative terms from the governing PDE, while the derivative terms from the governing PDE are approximated by the locally applied DQ method. Because of this, in the RDQ method, the derivative approximation accuracy is independent of the monomial order used in the fixed RKPM interpolation. This makes the RDQ method different from the collocation based strong-form methods, in which the derivative terms from the governing PDE are approximated by the shape function derivatives. As compared with the other weak-form methods, the RDQ method is capable of well capturing the local high gradients, which will be shown in Section 5.3.

Compared with the classical FEM, the merit of the RDQ method is that it can effectively handle the moving boundary problems, which is difficult for the FEM due to the problems of the mesh distortion and element singularities. In the RDQ method, the field nodes act as Lagrangian grid, and the virtual nodes act as Eulerian grid. The field nodes are free to move anywhere in the domain and no interconnectivity information among them is required. The virtual nodes are fixed in a space so that it is always possible to discretize the governing PDE by locally applying the DQ method over the virtual nodes.

This paper is organized as follows. The fixed RKPM is discussed in Section 2, the DQ and RDQ method formulations are given in Sections 3 and 4, respectively. The superconvergence condition is derived, and several test problems are solved using

the RDQ method, in Section 5. In Section 6, the RDQ method is applied to solve the fixed-fixed and cantilever beams for deflection due to the nonlinear electrostatic loading, and the conclusions are given in Section 7.

2 Fixed reproducing kernel particle method

In this section, the fixed RKPM interpolation function is discussed along with the cubic spline window function equation that will be used in the RDQ method.

The fixed RKPM interpolation function has several advantages over its classical, moving and the multiple fixed forms such as the partition of unity principle, constant moment matrix, and less computational efforts required. As per the fixed RKPM interpolation, function value approximation is given by,

$$f^h(x,y) = \int_{\Omega} C(x,y,u,v)\; K(x_k-u, y_k-v)\; f(u,v)\; du\; dv \tag{1}$$

where $f^h(x,y)$ is a function approximation of the function value $f(x,y)$ at a node (x,y), and $K(x_k-u,y_k-v)$ is a kernel function fixed at a node (x_k,y_k). The unknown correction functions, $C(x,y,u,v) = P^T(u,v)\; c(x,y)$, where $P^T(u,v) = \{b_1(u,v),\; b_2(u,v), ...,\; b$ is an m-order column vector of monomials, are determined by the consistency or reproducing condition. After simplifying, the shape functions are given as,

$$f^h(x,y) = \sum_{I=1}^{NP} N_I(x,y)\; u_I, \text{ where } I = 1 \text{ to } NP \text{ are interpolation nodes} \tag{2}$$

where, $N_I(x,y)$ and u_I are the fixed RKPM shape function and the field nodal parameters, respectively [Aluru (2000); Aluru and Li (2001)].

The kernel function, $K(x_k-u,y_k-v)$, is a window function normalized over a local domain such that it is nonzero within the local domain and zero outside of it,

$$K(x_k-u,y_k-v) = \frac{1}{d_x} w\left(\frac{x_k-u}{d_x}\right) \frac{1}{d_y} w\left(\frac{y_k-v}{d_y}\right) \tag{3}$$

where, d_x and d_y are the cloud sizes in the x and y directions, respectively. In the RDQ method, the cubic spline function is used as the window function,

$$w(z_I) = \begin{cases} 0, & z_I < -2 \\ \frac{1}{6}(z_I+2)^3, & -2 \le z_I \le -1 \\ \frac{2}{3} - z_I^2\left(1+\frac{z_I}{2}\right), & -1 \le z_I \le 0 \\ \frac{2}{3} - z_I^2\left(1-\frac{z_I}{2}\right), & 0 \le z_I \le 1 \\ \frac{-1}{6}(z_I-2)^3, & 1 \le z_I \le 2 \\ 0, & z_I > 2 \end{cases} \tag{4}$$

It is seen from Eq. (2) that $u_I \neq f^h(x,y)_I$ i.e. it does not have the delta function property. Thus, in the RDQ method, essential boundary conditions are imposed as explained in Section 4.

Jin, Li and Aluru (2001), and Atluri and Shen (2002) discussed the RKPM and MLS shape functions equivalence. Atluri and Shen (2002) shown that if the same kernel and the window functions are chosen in the RKPM and MLS, respectively, with the same consistency order, k, the resulting shape functions are identical.

3 Differential quadrature formulation

In the DQ method, the derivative terms in the governing PDE are approximated by the two approaches, the first by polynomials and the second by Fourier series. The polynomial based PDE discretization is adopted in the RDQ method.

In the polynomial based DQ, it is assumed that the function $f(x)$ is sufficiently smooth over a domain $[a,\ b]$ for N grid points, $x_1, x_2, ..., x_N$, so that its 1^{st}-order derivative, $f_x^{(1)}(x)$, at any node is approximated by,

$$f_x^{(1)}(x_i) = \sum_{j=1}^{N_x} a_{ij} f(x_j), \text{ for } i = 1,\ 2,\ ...,\ N_x \tag{5}$$

where, $f(x_j)$ is a function value at the point x_j, and a_{ij} are the 1^{st}-order derivative DQ weighting coefficients. The 2D function, $f(x,y)$, derivatives are approximated as,

$$f_x^{(1)}(x_i,y_j) = \sum_{k=1}^{N_x} a_{ik}^x f(x_k,y_j), \quad f_y^{(1)}(x_i,y_j) = \sum_{k=1}^{N_y} a_{jk}^y f(x_i,y_k) \tag{6}$$

where, a_{ik}^x and a_{jk}^y are the DQ weighting coefficients, and N_x and N_y are the total virtual nodes located inside the virtual node (x_i,y_j) local DQ domain in the x and y directions, respectively. Once the a_{ik}^x and a_{jk}^y weighting coefficients are determined, the numerical bridge to link the derivative terms from the governing PDE with the field node parameter values is established by approximating the virtual node function values by fixed RKPM interpolation. In the RDQ method, the DQ weighting coefficients are computed using Shu's general approach [Shu, Khoo and Yeo (1994)] as given,

$$a_{ik}^x = \frac{1}{x_i - x_k} \prod_{m=1, m\neq i,k}^{N_x} \left(\frac{x_i - x_m}{x_k - x_m}\right) \text{ and } a_{ii}^x = -\sum_{k=1_{k\neq i}}^{N_x} a_{ik}^x \tag{7}$$

Similar expressions can be written for a_{ik}^y and a_{ii}^y, the 1^{st}-order derivative DQ

weighting coefficients with respect to the y variable. The 2D case 2^{nd}-order derivative DQ discretization equations are given as,

$$f_x^{(2)}(x_i,\ y_j) = \sum_{k=1}^{N_x} b_{ik} f^h(x_k, y_j), \quad f_y^{(2)}(x_i,\ y_j) = \sum_{k=1}^{N_y} b_{jk} f^h(x_i, y_k)$$

and

$$f_{xy}^{(2)}(x_i,\ y_j) = \sum_{l=1}^{N_x} a_{il} \sum_{k=1}^{N_y} a_{jk} f^h(x_l, y_k) \tag{8}$$

where,

$$b_{ik} = 2a_{ik}\left[a_{ii} - \frac{1}{x_i - x_k}\right] \text{ for } i \neq k, \quad b_{ii} = -\sum_{k=1_{k\neq i}}^{N_x} b_{ik} \text{ for } i = k \tag{9}$$

Recurrent formula for higher order weighting coefficients is given by Shu (2000).

4 The RDQ method

The main limitation of the DQ method to have all collinear field nodes is overcome in RDQ method. The field nodes are created in the uniform or random manner. The virtual nodes are created by cosine distribution,

$$x_i = x_0 + \frac{L}{2}\left[1 - \cos\left(\frac{i-1}{N-1}\pi\right)\right], \text{ for } i = 1,\ 2,\ ...,\ N \text{ virtual nodes} \tag{10}$$

where x_0 and L are the starting co-ordinate and domain length, respectively. As per Runge phenomenon, with increase in the field variable interpolation order by the uniform node distribution, the numerical solution gets unstable across the domain boundaries. This can be avoided if the nodes are distributed densely near the boundaries and progressively become uniform with in the domain. This requirement is fulfilled by Chebyshev nodes. Chebyshev polynomials of the 1^{st}-kind [Christoph (1997); Sarra (2006)] are the roots of 2^{nd}-order Chebyshev differential equation, whose roots are called as Chebyshev nodes or Chebyshev-Gauss-Lobatto (CGL) points. As the CGL points, $x_k = -\cos\left[((k-1)/(N-1))\,\pi\right]$, for $k = 1,\ 2,\ ...,\ N$, cover the domain boundaries ± 1, it is easy to impose the essential boundary conditions. Eq. (10) is the CGL node equation applied over domain $[x_0,\ (x_0 + L)]$.

4.1 Function value Interpolation and the DQ domain creation

The field variable interpolation domain is created around each virtual node as shown in Fig. 1. The field nodes falling in it are taken into consideration for

the function value approximation at that virtual node by the fixed RKPM interpolation function. Any local domain shape can be considered like a circle or rectangle; the circular shape is adopted in the RDQ method. Let $d_x = \alpha_x \Delta_x$ and $d_y = \alpha_y \Delta_y$ be the domain sizes in the x and y directions, respectively [Aluru and Li (2001)], where, Δ_x and Δ_y are nodal spacings in the x and y directions, respectively. The nodal spacings are easily computed for the uniform field node distribution but for the random field nodes, it is done while computing the shape functions by taking the nodal co-ordinates average. The α_x and α_y define the local domain sizes in the x and y directions, respectively. Two approaches are studied to define α_x and α_y. As per the first approach, the positivity condition is derived based on the fact that the fixed RKPM interpolation kernel function is nonzero only over a certain local domain. As per Eq. (4), the kernel function will be zero if $z_I > 2$ or $z_I < -2$, which means that α_x and α_y should have the values such that $z_I < 2$ or $z_I > -2$,

$$\frac{(x_k - x_i)}{\alpha_x \Delta_x} \geq -2 \text{ and } \frac{(x_k - x_i)}{\alpha_x \Delta_x} \leq 2 \tag{11}$$

$$\alpha_x \in \left[\left(\frac{x_k - x_i}{2\Delta_x} \right), - \left(\frac{x_k - x_i}{2\Delta_x} \right) \right] \text{ for the domain } [2, \ -2] \tag{12}$$

where, i and k refers the field and virtual nodes, respectively. The highest absolute α_x is selected from all the values obtained by Eq. (12). In the second approach, an extensive numerical analysis is carried out and found out that for a function convergence, $\alpha_x = 2.23$ (for 1D) and $\alpha_x = 1.17$ (for 2D) gives good results. $\alpha_x = 1.17$ is adopted for a presented work [Aluru and Li (2001)].

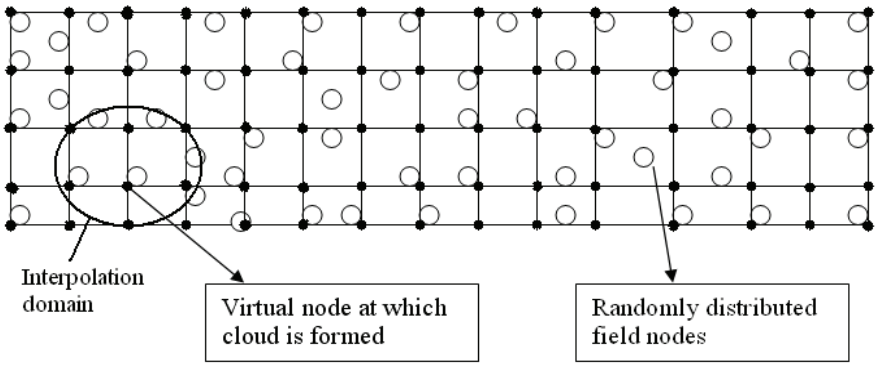

Figure 1: Virtual and field node distributions and the fixed RKPM interpolation local domain creation around the virtual nodes.

The local DQ domain is created around each virtual node in the x and y directions and the virtual nodes falling in it are considered for the locally applied DQ approximation at that virtual node as shown in Fig. 1. A function value at each virtual node is approximated by the interpolation domain created earlier by the fixed RKPM interpolation as,

$$f^h(x_i,\ y_j) = \sum_{k=1}^{NP} N_k(x_i,y_j)\ u_k \tag{13}$$

where $N_k(x_i,y_j)$ are the shape functions at NP field nodes located in the local domain around the virtual node (x_i,y_j), $f^h(x_i,y_j)$ is the function approximation at virtual node (x_i,y_j), and u_k are the nodal parameters. The governing PDE is discretized at all the internal virtual nodes, Dirichlet and Neumann boundary conditions are imposed at the boundary virtual nodes in the strong form by the RDQ method. All the boundary condition equations are combined with the governing PDE discretization equations to get the global equations matrix.

4.2 Imposing Dirichlet boundary conditions

Dirichlet boundary conditions are imposed in the strong form at boundary virtual nodes by assuming $u_I = f^h(x,y)_I$. For example, if the 1^{st} and 4^{th} virtual nodes are on Dirichlet boundary, the modified stiffness matrix is given as,

$$\begin{bmatrix} 1 & 0 & 0 & 0 \\ k_{21} & k_{22} & k_{23} & k_{24} \\ k_{31} & k_{32} & k_{33} & k_{34} \\ 0 & 0 & 0 & 1 \end{bmatrix} \begin{Bmatrix} u_1 \\ u_2 \\ u_3 \\ u_4 \end{Bmatrix} = \begin{Bmatrix} b_1 \\ F_2 \\ F_3 \\ b_4 \end{Bmatrix} \tag{14}$$

thus, u_1 and u_4 are computed as b_1 and b_4, respectively.

4.3 Solving final system of equations

It is necessary to have the virtual nodes at least equal to the field nodes to get the unique solution; the solution is improved as the virtual nodes are increased. Suppose the final system of equations is $K_{mxn}U_{nx1} = F_{mx1}$, where $m > n$; to get a square K matrix, it is solved in a least square sense by multiplying K^T on both sides to get $K'_{nxn}U_{n\times 1} = F'_{nx1}$. Thus, the solution vector is computed by minimizing the residual error $(K'U - F')$. As the fixed RKPM interpolation function does not have a delta function property, the field node function values are computed by interpolating each field node by the surrounding field nodes by Eq. (13).

4.4 Approximate derivatives computation

A novel approach called the weighted derivatives approach is formulated to compute the approximate derivative values at all field nodes such that the 1^{st}- and 2^{nd}-order derivatives with respect to the x variable at node (x_k) are given as,

$$f(x_k)_{,x} = \sum_{i=1}^{NP} N_i(x_k)\ f(x_i)_{,x} \text{ and } f(x_k)_{,xx} = \sum_{i=1}^{NP} N_i(x_x)\ f(x_i)_{,xx} \tag{15}$$

where x_i are the field nodes in the field node, x_k, interpolation domain, and $f(x_i)_{,x} = \frac{f(x_i)-f(x_k)}{(x_i-x_k)}$, $f(x_i)_{,xx} = \frac{f(x_i)_{,x}-f(x_k)_{,x}}{(x_i-x_k)}$ and $N_i(x_k)$ are the 1^{st}- and 2^{nd}-order approximate derivatives, and the shape function values at the i^{th} node, respectively. Eqs. (5) and (8) are not related with Eq. (15), as they are utilized to approximate the derivative terms from governing PDE while discretizing it at the internal virtual nodes, where as Eq. (15) is used to compute the field node approximate derivative values after computing the nodal parameter values. The expressions similar to Eq. (15) can be written for the y variable derivatives.

4.5 Convergence rate computation

The convergence rates for all the presented problems are computed by [Mukherjee and Mukherjee (1997); Aluru and Li (2001)],

$$\varepsilon = \frac{1}{|f^e|_{\max}} \sqrt{\frac{1}{NP} \sum_{I=1}^{NP} \left[f_I^{(e)} - f_I^{(n)} \right]^2} \tag{16}$$

where ε is a global error in the solution, $f_I^{(e)}$ and $f_I^{(n)}$ are I^{th} field node exact and numerical function values, respectively, and NP are the total field nodes.

In order to compute the global error and convergence rates for randomly scattered field nodes, first the random field node function values are computed by the RDQ method. The solution is then approximated over the equal number of uniformly distributed points [Aluru (2000)] by the random field node function values. The function values, and the 1^{st}- and 2^{nd}-order derivatives are computed for these uniform points and the convergence curves are plotted by the nodal spacings given as [Aluru (2000); Aluru and Li (2001)],

$$h = h_x = h_y = \frac{length}{\sqrt{NP}-1}, \text{ where } NP \text{ is the total random field nodes} \tag{17}$$

where, h_x and h_y are nodal spacings in the x and y directions, respectively, for the uniformly distributed points, and $length$ is a domain length.

5 Convergence analysis

It is observed that the solution accuracy is affected by the ratio of field and virtual nodes. In order to identify their relation, an analytical condition, called the superconvergence condition, is derived which correlate the number of field and virtual nodes. The RDQ method numerical accuracy is studied using the superconvergence condition by solving several test problems. All the convergence rates are computed using the global errors obtained by Eq. (16).

5.1 The superconvergence condition

Let N_v and N_r be the number of field and virtual nodes, respectively, distributed in a computational domain. In order to identify the relationship between them, for a given problem, it is supposed that two graphs are plotted viz. $\ln(E)$ versus $\ln(h_r)$ and $\ln(E)$ versus $\ln(h_r h_v)$ where, E is a global error, and h_r and h_v are the field and virtual node spacings, respectively; let m_1 and m_2 be the slopes of these graphs, respectively. The m_1 and m_2 equations can be written as,

$$\ln(E) = m_1 \ln(h_r) \text{ and } \ln(E) = m_2 \ln(h_r/h_v) \tag{18}$$

$$\frac{m_1}{m_2} = \frac{\ln(h_r/h_v)}{\ln(h_r)} \tag{19}$$

$N_v \geq N_r$ for a unique solution, and $h_r = L/(N_r - 1)$ and $h_v = L/(N_v - 1)$ where, L is a domain length. It can be stated by observation that $\ln(h_r)$ has a zero or negative value as $h_r \leq 1$, $\ln(h_r/h_v)$ always has a zero or positive value as $h_r \geq h_v$, and $\ln(E)$ has either a positive or negative value as $E > 0$ or $E < 0$. Based on this input, four conditions are possible for the m_1, m_2 and m_1/m_2 signs. Careful consideration of these four conditions results in only one valid possibility as given in Tab. 1,

Table 1: Different possibilities of m_1, m_2 and m_1/m_2 signs

m_1	m_2	m_1/m_2	Is valid?
+ve	+ve	+ve	No
+ve	-ve	-ve	Yes
-ve	-ve	+ve	No
-ve	+ve	-ve	No

Thus, m_1, m_2 and m_1/m_2 should have +ve, -ve and -ve signs, respectively. For the different numbers of field nodes and fixed number of virtual nodes, m_2 is not a constant but has a different value at each h_r/h_v location. Thus, in order to maintain a constant $\lambda = (m_1/m_2)$ value with respect to different N_r values, the 3^{rd} graph,

(λ) versus (h_r), is plotted. The origin of (λ) versus (h_r) graph is at $(h_v,\ 0)$ as the lowest values of $h_r = h_v$ and $\lambda = 0$. The slope of the third graph with respect to the origin and using any two points on the graph, $(\lambda_1,\ h_{r1})$ and $(\lambda_2,\ h_{r2})$, can be as,

$$\lambda_1 - 0 = h_{r1} - h_v \text{ and } \lambda_2 - 0 = h_{r2} - h_v \tag{20}$$

$$\frac{\lambda_1}{\lambda_2} = \frac{(h_{r1} - h_v)}{(h_{r2} - h_v)} \tag{21}$$

for a fixed m_1 value, Eq. (21) is simplified as,

$$\frac{(m_2)_2}{(m_2)_1} = \frac{(h_{r1} - h_v)}{(h_{r2} - h_v)} \tag{22}$$

If the m_1 and λ values are fixed, the successive m_2 values can be computed and by further fixing h_v and h_{r1} values, the successive h_{r2} values can be computed by Eq. (22). If a test problem is solved using these successive h_r values (corresponding to fixed m_1 value) and a fixed N_v value hence, as per Eq. (22), m_1 convergence rate should be achieved. Thus, it shows that if a test problem is solved using the field nodes obtained by Eq. (22) and approximating a function value by up to p order monomials, a convergence rate higher than $o\left(h^{p+1}\right)$ is possibly obtained. Therefore, Eq. (22) is called as the superconvergence condition. The application of Eq. (22) is demonstrated in Sections 5.2 and 5.3 by solving several 1D and 2D test problems, respectively.

The approximate field node function derivatives are computed by the weighted derivatives approach as explained in Section 4.4, the numerical error in the computed derivatives is more than the corresponding function values. In order to obtain a good convergence, it is essential to ensure that the derivative error norm reduces as we increase the field nodes. In order to achieve this thus, the complete or Sobolev error norm is computed after applying Eq. (22),

$$(E)_0 = \sqrt{\sum_{I=1}^{N_r} (f^e - f^n)^2}, \text{ Sobolev norm of the order 0} \tag{23}$$

$$(E)_1 = (E)_0 + \sqrt{\sum_{I=1,\ j=1}^{N_r,\ 3} \left[\left(\frac{\partial f}{\partial x_j}\right)^e - \left(\frac{\partial f}{\partial x_j}\right)^n\right]^2}, \text{ Sobolev norm of the order 1} \tag{24}$$

where $(E)_0$ and $(E)_1$ are 0^{th} and 1^{st} order Sobolev error norms, respectively, and e and n are the exact and numerical values, respectively. It is seen from Eq. (24) that as the square of the error in the function and its corresponding derivative values is added, the $(E)_0$ term contribution to the $(E)_1$ term becomes less as compared with the derivatives error term. Hence, with the successively increasing field nodes and if $(E)_1$ reduces, then actually the derivatives error term reduces. Thus, Sobolev or complete error norm computed by Eq. (24) can be fairly taken as an indicator of the reduction in the derivatives error at the field nodes.

5.2 1-D problems

The first 1D problem is a Poisson equation with a constant force term. Its governing equation and boundary conditions are given as,

$$\frac{d^2f}{dx^2} = 2, \quad (0 < \mathrm{x} < 8) \text{ and } f(x=0) = 0, \quad f(x=8) = 64 \tag{25}$$

The exact solution is given as $f(x) = x^2$. This problem is solved by including the 2^{nd}-order monomials in the function approximation polynomial basis, and using 6, 21, 161, 321 field and 460 virtual nodes. The convergence curves are plotted in Fig. 2 and it is seen that the convergence values obtained by the random field nodes are equally good as uniform field nodes. The analytical and numerical function value comparisons are given in Fig. 3.

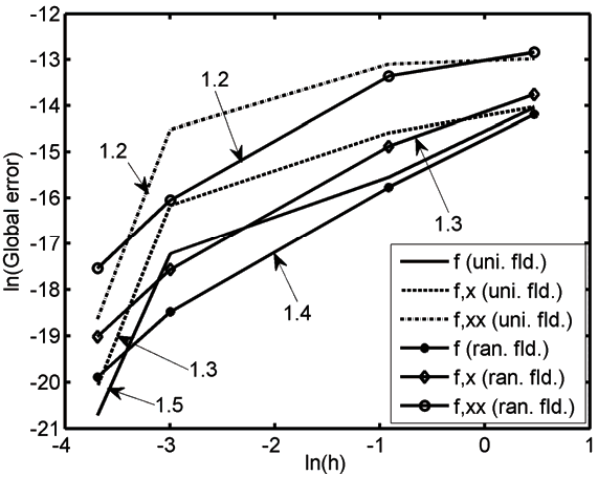

Figure 2: Convergence plots for the first 1D problem of Poisson equation by the uniform and random field node distributions.

The second 1D problem is a mixed boundary value problem with the analytical solution containing the 4^{th}-order monomial therefore; it is interesting to see how the RDQ method converges by including the 2^{nd}-order monomials. Its governing equation and boundary conditions are as,

$$\frac{d^2f}{dx^2} = \frac{105}{2}x^2 - \frac{15}{2}, \quad (-1 < \mathrm{x} < 1) \text{ and } f(x=-1) = 1, \quad \frac{df}{dx}(x=1) = 10 \quad (26)$$

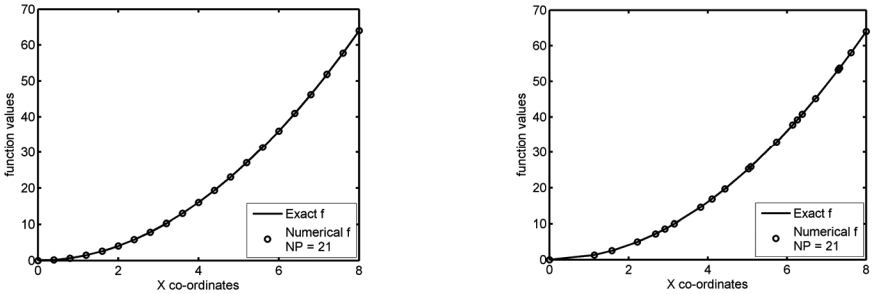

Figure 3: Function values comparison for the 1^{st} 1D problem of Poisson equation using a) uniform and b) random field nodes, respectively.

The analytical solution is given as $f(x) = 35/8x^4 - 15/4x^2 + 3/8$. This problem is solved by the superconvergence condition with m_1 = 3, $N_v = 641$, $h_{r1} = 0.05$ and $\lambda_1 = -1.2$. The successive λ values are obtained by dividing the λ_1 value by 3 and using Eq. (22) to compute the corresponding h_{r2} values. As such, $N_r = 58$, 145, 299, 464, 569, and 632 are obtained. In order to compare the results, this problem is also solved by 2^{nd} set of 21, 41, 81, 161, 321, 641 field and 641 virtual nodes, respectively. The convergence curves obtained by both field node sets are plotted in Figs. 4a and 4b and the corresponding convergence rates are given in Tab. 2. It is seen from Tab. 2 that all the convergence values obtained by the field nodes computed by Eq. (22) are improved, the derivative convergence values are superconvergent, and the function value convergence by the random field nodes is also superconvergent. Fig. 5a shows the reduction in the complete Sobolev norm up to order 2 by the superconvergence condition field nodes. This problem is also solved by the 4^{th}-order monomials; the convergence curves are given in Fig. 5b. When Tab. 2 and Fig. 5b are compared, it is observed that the derivative convergence values are considerably improved and the random field nodes convergence values are almost equal to or better than by the uniform nodes. This indicates that the RDQ method is capable of equally handling the uniform and random node

distributions, which is one of the objectives of its development. The analytical and numerical solution comparison curves are given in Fig. 6. From all the results it is seen that quite good function and its 1^{st}- and 2^{nd}-order derivatives convergence rates are achieved by the RDQ method with the domain discretized by uniform and the random field nodes.

It is observed from Tab. 2 that the convergence rates obtained by the superconvergence condition are improved and the derivatives values are superconvergent. It is seen from Fig. 5b that the RDQ method converges at the faster rate with increase in the function approximation monomial order.

Table 2: Convergence rates for the 2^{nd} 1D problem using up to 2^{nd}-order monomials

function	for 2^{nd} set (uni. nodes)	superconvergence (uniform nodes)	for 2^{nd} set (ran. nodes)	Superconvergence (random nodes)
f	1.7	3.0	1.8	3.8
$f_{,x}$	0.9	1.8	0.8	2.1
$f_{,xx}$	0.9	1.2	0.7	1.4

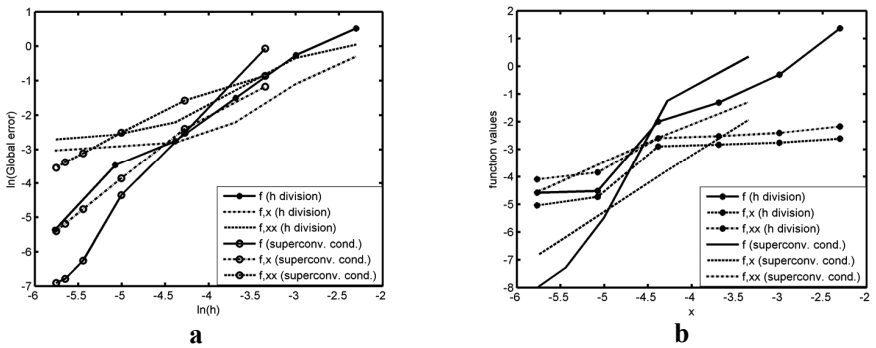

Figure 4: Convergence curves for the 2^{nd} 1D problem of Poisson equation by a) uniform and b) random field nodes, respectively. The curves are plotted using field nodes obtained by uniformly decreasing h and by the superconvergence condition.

The third 1D problem is having a local high gradient. This problem is solved by the 2^{nd}-order monomials. Its governing equation and boundary conditions are given as,

$$\frac{d^2f}{dx^2} = -6x - \left[\left(\frac{2}{\alpha^2}\right) - 4\left(\frac{x-\beta}{\alpha^2}\right)^2\right] \exp\left[-\left(\frac{x-\beta}{\alpha}\right)^2\right] \quad (0 < x < 1) \tag{27}$$

$$f(x=0)=\exp\left[-\left(\frac{\beta^2}{\alpha^2}\right)\right], \quad \frac{df(x=1)}{dx}=-3-2\left(\frac{1-\beta}{\alpha^2}\right)\exp\left[-\left(\frac{1-\beta}{\alpha}\right)^2\right] \tag{28}$$

Its analytical solution is given as $f(x)=-x^3+\exp\left[-((x-\beta)/\alpha)^2\right]$. This problem is solved using the superconvergence condition by fixing $m_1=2$, $N_v=641$, $h_{r1}=0.05$ and $\lambda_1=-1.2$. The successive λ values are obtained by dividing the λ_1 by 2 and using Eq. (22) to compute the corresponding h_{r2} values.

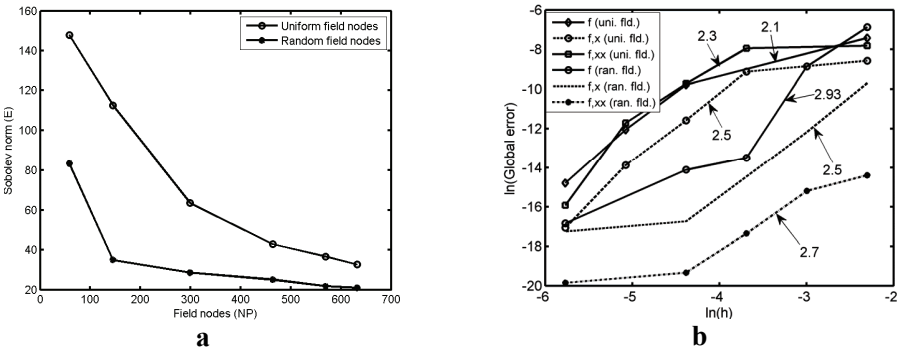

Figure 5: For the 2^{nd} 1D problem, a) reduction in the complete error norm with increasing the field nodes obtained by superconvergence condition b) convergence plots by the uniform and random field nodes, with the 4^{th}-order monomials.

Hence, $N_r=21,\ 40,\ 75,\ 133,\ 219,\ 327,\ 433,\ 517$ and 572 are obtained. The convergences are given in Fig. 7 and it is noted that the uniform field nodes function value convergence is $O\left(h^{p+2.1}\right)$ and all the derivatives convergence values are also superconvergent, Sobolev error norm is plotted in Fig. 8.

5.3 2-D problems

The first 2-D problem is a Laplace equation with Dirichlet boundary conditions as,

$$\nabla^2 f=0,\ (0<x<1) \text{ and } (0<y<1) \tag{29}$$

$$f(x=0,y)=-y^3, \quad f(x=1,y)=-1-y^3+3y^2+3y \tag{30}$$

$$f(x,y=0)=x^3, \quad f(x,y=1)=-1-x^3+3x^2+3x \tag{31}$$

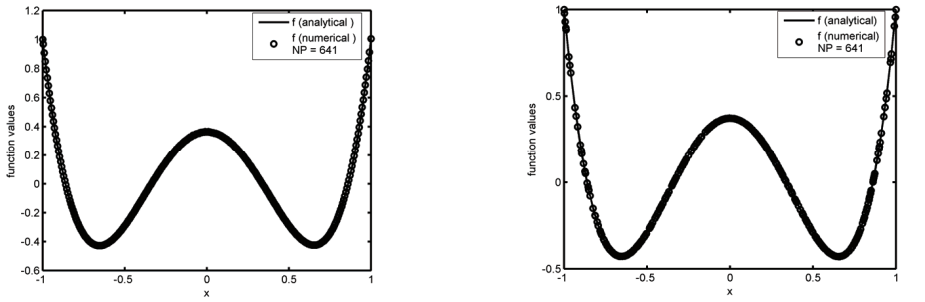

Figure 6: Numerical and analytical function values comparison for the 2^{nd} 1D problem by a) uniform and b) random field nodes, respectively

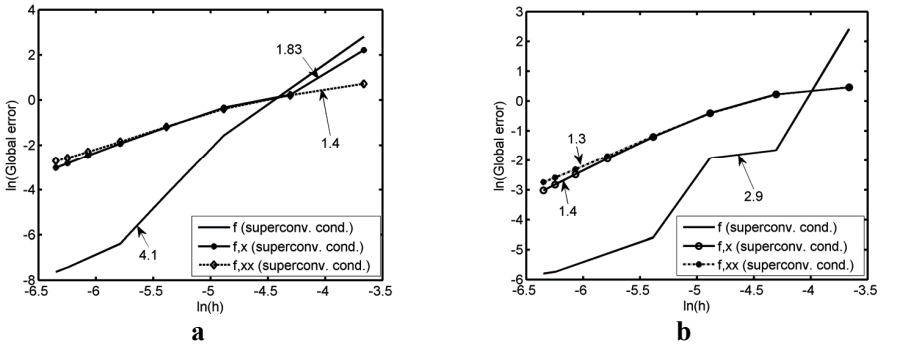

Figure 7: Convergence curves for the 3^{rd} 1D problem of local high gradient by a) uniform and b) random field nodes, respectively.

Analytical solution is given as $f(x,y) = -x^3 - y^3 + 3xy^2 + 3x^2y$. The problem is solved with the 2^{nd}-order monomials, and 5×5, 9×9, 17×17, 33×33, 44×44 field and 44×44 virtual nodes. The convergence curves are plotted in Figs. 9a and 9b, and it is observed that better function convergence is achieved by the random field nodes but the derivatives convergence remain unchanged. The analytical and numerical function values comparison plots are given in Figs. 10a and 10b.

The 2^{nd} 2-D problem is also Laplace equation with mixed boundary conditions as,

$$\nabla^2 f = 0\ ,\ (0 < x < 1) \text{ and } (0 < y < 1) \tag{32}$$

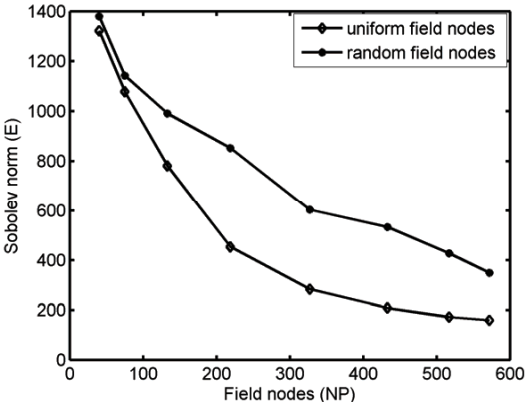

Figure 8: Reduction in the Sobolev error norm for the 3^{rd} 1D problem.

$$f(x=0,y)=-y^3, \quad f(x=1,y)=-1-y^3+3y^2+3y \tag{33}$$

$$\frac{df}{dy}(x,y=0)=3x^2, \quad \frac{df}{dy}(x,y=1)=-3+6x+3x^2 \tag{34}$$

Analytical solution is given as, $f(x,y)=-x^3-y^3+3xy^2+3x^2y$. This problem

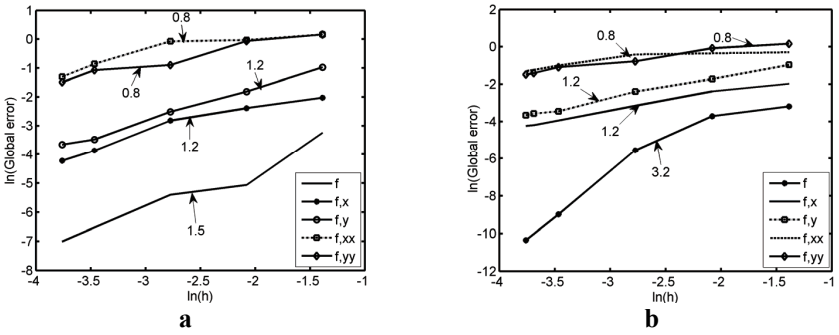

Figure 9: Convergence curves for the 1^{st} 2D problem of Laplace equation by a) uniform and b) random field nodes, respectively, by the 2^{nd}-order monomials.

is solved with the 2^{nd}-order monomials, and 5×5, 9×9, 17×17, 33×33, 41×41,

44×44 field and 44×44 virtual nodes. The convergence curves are plotted in Figs. 11a and 11b and it is observed that better function convergence is achieved by the random field nodes.

The third 2-D problem solved is of local high gradient value at node (0.5, 0.5). Its governing equation and the boundary conditions are given as,

$$\nabla^2 f = -6x - 6y - \left[\left(\frac{4}{\alpha^2}\right) - 4\left(\frac{x-\beta}{\alpha^2}\right) - 4\left(\frac{y-\beta}{\alpha^2}\right)\right] \times$$

$$\exp\left[-\left(\frac{x-\beta}{\alpha}\right)^2 - \left(\frac{y-\beta}{\alpha}\right)^2\right], (0 < x < 1) \text{ and } (0 < y < 1) \tag{35}$$

$$f(x=0,y) = -y^3 + \exp\left[-\left(\frac{\beta}{\alpha}\right)^2 - \left(\frac{(y-\beta)}{\alpha}\right)^2\right] \tag{36}$$

$$f(x=1,y) = -1 - y^3 + \exp\left[-\left(\frac{(1-\beta)}{\alpha}\right)^2 - \left(\frac{(y-\beta)}{\alpha}\right)^2\right] \tag{37}$$

$$\frac{df}{dy}(x, y=0) = \frac{2\beta}{\alpha^2}\exp\left[-\left(\frac{\beta}{\alpha}\right)^2 - \left(\frac{(x-\beta)}{\alpha}\right)^2\right] \tag{38}$$

$$\frac{df}{dy}(x, y=1) = -3 - 2\left(\frac{(1-\beta)}{\alpha^2}\right)\exp\left[-\left(\frac{(x-\beta)}{\alpha}\right)^2 - \left(\frac{(1-\beta)}{\alpha}\right)^2\right] \tag{39}$$

The analytical solution is given as,

$$f(x,y) = -x^3 - y^3 + \exp\left[-((x-\beta)/\alpha)^2 - ((y-\beta)/\alpha)^2\right].$$

This problem is solved with the 2^{nd}-order monomials and the superconvergence condition by fixing $m_1 = 2, N_v = 44 \times 44, h_{r1} = 0.25$ and $\lambda_1 = -1.2$. The successive λ values are obtained by dividing the λ_1 by 2 and using Eq. (22) to compute the h_{r2} values. Thus, $N_r = 5 \times 5$, 9×9, 13×13 and 19×19 are obtained. The convergence curves are plotted in Figs. 12a and 12b and it is observed that the derivative convergence values are superconvergent in nature. Fig. 13 shows the numerical and analytical function values comparison.

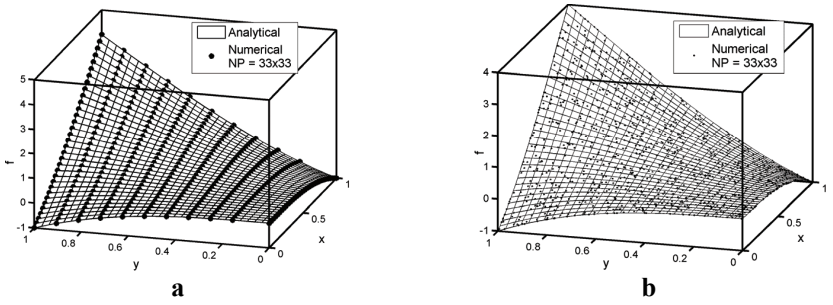

Figure 10: Numerical and analytical function values comparison for 1^{st} 2D problem of Laplace equation by 33×33 a) uniform b) random field nodes, respectively.

The 4^{th} 2D problem is of steady-state heat conduction in a rectangular plate domain with a heat source. Its governing equation and boundary conditions are as,

$$\nabla^2 T = -2\, s^2 \operatorname{sec h}^2 [s(y-0.5)] \tanh[s(y-0.5)], (0<x<0.5),\ (0<y<1) \tag{40}$$

$$\frac{\partial f}{\partial n} = 0 \text{ along } x = 0 \text{ and } 0.5, \quad T(y=0) = -\tanh\left(\frac{s}{2}\right), \quad T(y=1) = \tanh\left(\frac{s}{2}\right) \tag{41}$$

The successive λ values are obtained by dividing the λ_1 by 3 and using Eq. (22) to compute the corresponding h_{r2} values. As a result, $N_r = 6\times6,\ 13\times13,\ 21\times21$ and 28×28 are obtained. The temperature and its gradient convergence plots are given in Fig. 14a and the corresponding convergence values are 3.2 and 2.4. The Sobolev norm plot with increasing field nodes, and the numerical and analytical temperature comparisons are given in Figs. 14b and 15, respectively.

It is seen from Fig. 14a that good function and derivative convergences are achieved by the superconvergence condition field nodes. The superconvergent derivative values confirm that the weighted derivatives approach gives very good results.

5.4 Elasticity problems

All problems are solved for plane stress condition with the governing equation as,

$$\sigma_{i,j} + B_i = 0 \tag{42}$$

where, σ_i and B_i are the stresses and body forces in the i^{th} direction, respectively.

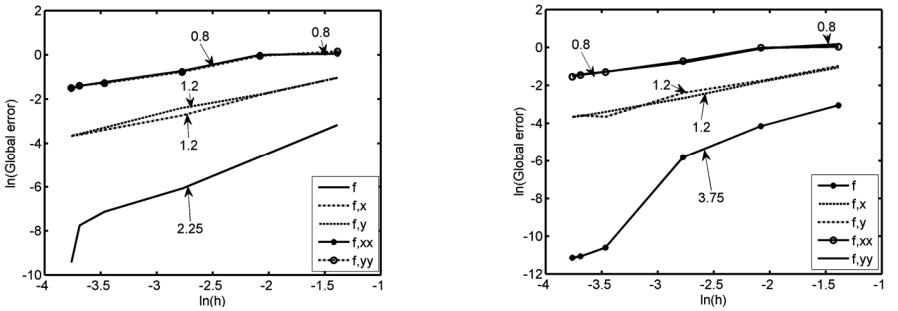

Figure 11: Convergence plots for the 2^{nd} 2D problem of Laplace equation by a) uniform b) random field nodes, respectively.

5.4.1 Cantilever beam under pure bending

A cantilever beam under the bending load is shown in Fig. 16a. The analytical solutions are derived as [Timoshenko and Goodier (1970), and Zhilun (1992)],

$$u = \frac{M}{EI}xy, \quad v = \frac{-\nu_0 M}{2EI}y^2 - \frac{M}{2EI}x^2 \text{ and } \sigma_x = \frac{My}{I},\ \sigma_y = 0,\ \sigma_{xy} = 0 \tag{43}$$

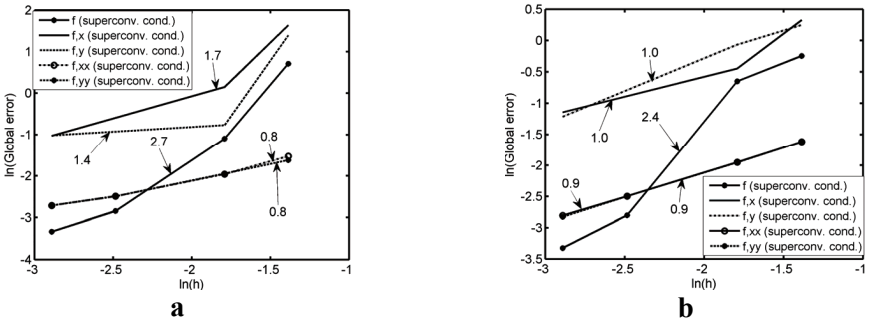

Figure 12: Convergence plots for the 3^{rd} 2D problem of local high gradient by a) uniform b) random field node distributions, respectively.

This problem is solved for $L = 48$, $D = 12$, $M = -24000$, $\nu_0 = 0.3$, $E = 3.0 \times 10^{07}$, and 13×13, 17×17, 21×21, 29×29 field and 41×41 virtual nodes, with the 1^{st}-order monomials in the function approximation. The u and v displacement convergence rates, by discretizing the domain with uniform and the random field nodes,

are given as 1.0 and 1.3, and 1.96 and 2.0, respectively, corresponding convergence plots are given in Fig. 16b. When this problem is solved by 9×9 uniform field and 41×41 virtual nodes with the 2^{nd}-order monomials, the analytical solutions are almost exactly reproduced with the u and v displacements global error values as 3.53×10^{-13} and 2.54×10^{-12}, respectively.

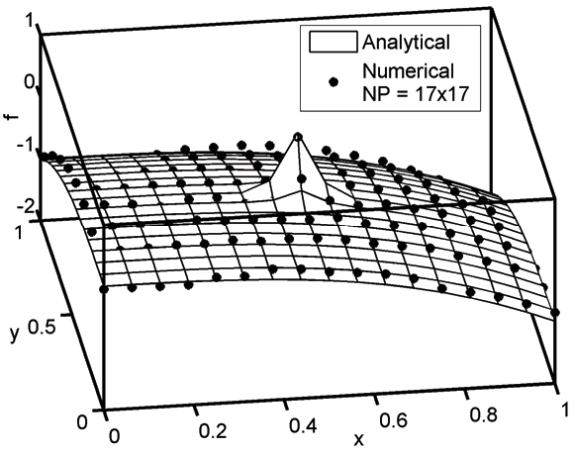

Figure 13: The numerical and analytical function values comparison for the third 2-D problem of local high gradient using the uniform field node distribution.

5.4.2 Cantilever beam under pure shear

A cantilever beam loaded under the pure shear is shown in Fig. 17a with stresses as,

$$\sigma_{xx} = \frac{P(L-x)y}{I}, \quad \sigma_{xy} = \frac{-P}{2\,I}\left(\frac{D^2}{4} - y^2\right) \text{ and } \sigma_y = 0 \tag{44}$$

The analytical solutions are derived as [Timoshenko and Goodier (1970), and Zhilun (1992)],

$$u = \frac{Pyx}{EI}\left(L - \frac{x}{2}\right) - \frac{\nu_0 P y^3}{6EI} + \frac{Py^3}{6GI} - \frac{PD^2 y}{8GI},\; v = \frac{-\nu_0 P y^2 (L-x)}{2EI} - \left(\frac{Px^2}{EI}\right)\left(\frac{L}{2} - \frac{x}{6}\right) \tag{45}$$

where, $G = E/2\,(1+\nu_0)$, $I = D^3/12$ (beam has a unit thickness). This problem is solved for $L = 48$, $D = 12$, $P = -1000$, $\nu_0 = 0.3$, $E = 3.0\times10^{07}$, and 13×13,

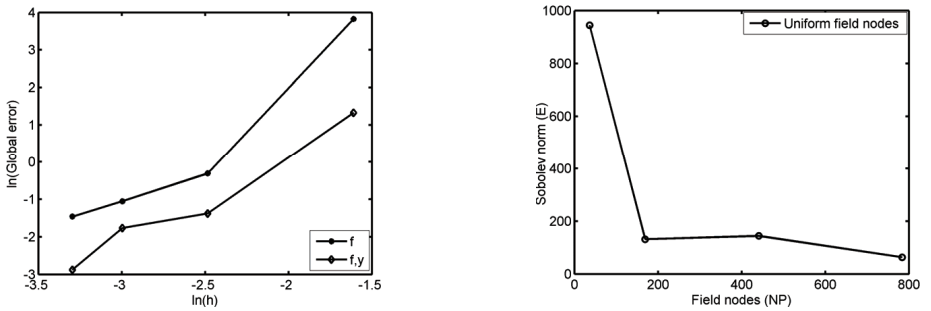

Figure 14: For the 4^{th} 2D problem of steady-state heat conduction a) convergence plots using uniform field nodes, b) reduction in Sobolev norm with field nodes.

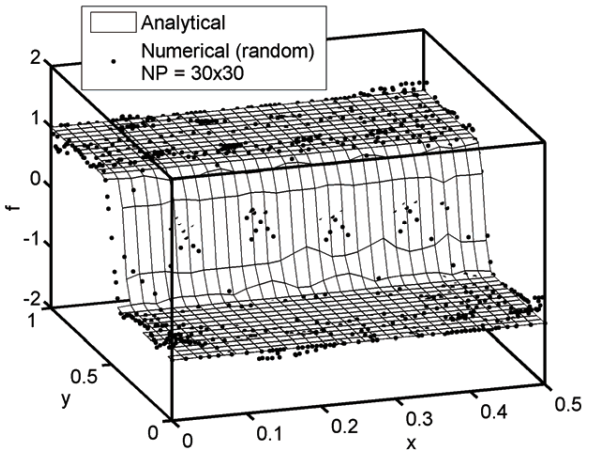

Figure 15: Temperature distribution within the domain.

17×17, 21×21, 29×29 field and 41×41 virtual nodes, with the 2^{nd}-order monomials. The u and v displacement convergence rates by the uniform and random field nodes are 1.94 and 1.9, and 1.5 and 2.0, respectively; the corresponding convergence curves are plotted in Fig. 17b. When this problem is solved by 9×9 field and 41×41 virtual nodes with 1^{st}-, 2^{nd}- and 3^{rd}-order monomials, the numerical results are steadily improved as shown in Tab. 3.

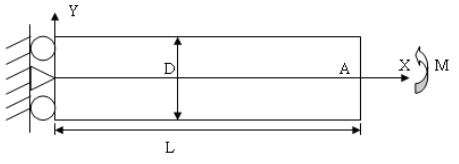

a

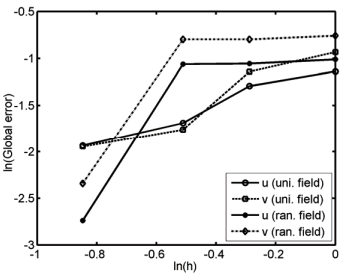

b

Figure 16: For a cantilever beam under pure bending load a) schematic of a cantilever beam under a pure bending load, b) u and v displacement convergence plots by the uniform and random field nodes.

Table 3: Decrease in the global error values with increase in the monomial order

Monomial order	Global error in u	Global error in v
1	1.38×10^{-04}	1.2
2	3.78×10^{-05}	5.03×10^{-02}
3	3.26×10^{-09}	2.43×10^{-09}

5.4.3 Semi infinite plate with central hole

The RDQ method is applied to solve a semi-infinite plate with a central hole. Due to the symmetric boundary value problem, only one quarter of the plate is used as the computation domain as shown in Fig. 18a. The analytical solutions in Cartesian co-ordinate system are given as,

$$u = \left(\frac{1+\nu_0}{E}\right) P \left[\frac{r}{1+\nu_0}\cos\theta + \left(\frac{2}{1+\nu_0}\right)\frac{b^2}{r}\cos\theta + \frac{b^2}{2\,r}\cos(3\theta) - \frac{b^4}{2\,r^3}\cos(3\theta)\right] \quad (46)$$

$$v = \left(\frac{1+\nu_0}{E}\right) P \left[\left(\frac{-\nu_0\, r}{1+\nu_0}\right)\sin\theta - \left(\frac{1-\nu_0}{1+\nu_0}\right)\frac{b^2\,\sin\theta}{r} + \frac{b^2\,\sin(3\theta)}{2\,r} - \frac{b^4\,\sin(3\theta)}{2\,r^3}\right] \quad (47)$$

where, r and θ are the local polar co-ordinates at each field node. Along 2, all the traction components are equal to zero i.e.

$$\sigma'_{xx} = n_x t_x + n_y t_y = 0 \text{ and } \sigma'_{xy} = -n_y t_x + n_x t_y = 0 \tag{48}$$

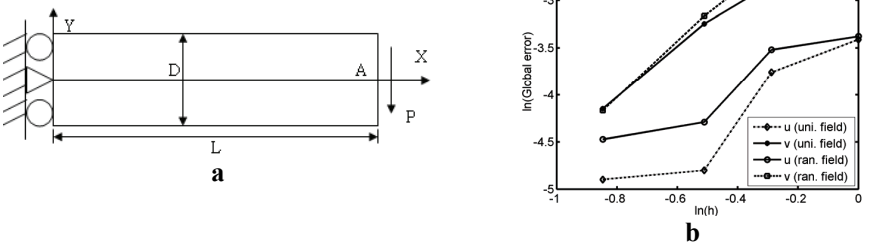

Figure 17: For a cantilever beam under pure shear load a) schematic of a cantilever beam under a pure shear load, b) u and v displacement convergence plots by the uniform and random field nodes.

where, $t_x = n_x\sigma_{xx} + n_y\sigma_{xy}$ and $t_y = n_x\sigma_{yx} + n_y\sigma_{yy}$, n_x and n_y are the direction cosines in the x and y directions, respectively. The problem is solved for $a = 1$, $b = 5$, $P = 1$, $\nu_0 = 0.3$ and $E = 1000$, and 6×6, 11×11, 21×21, 31×31 uniform field and 34×34 virtual nodes, with the 2^{nd}-order monomials. The u and v displacement convergence values by the uniform field nodes are obtained as 0.3, 0.3, respectively, and the convergence curves are plotted in Fig. 18b. Along the boundary 1, the numerical and analytical σ_{xx} values are given in Fig. 19.

6 Application of the RDQ method in solving the fixed-fixed and cantilever beams under the nonlinear electrostatic loading

In this section, the RDQ method is tested for the 4^{th}-order field variable reproducibility by solving the fixed-fixed and cantilever beams, as shown in Figs. 20a and 20b, respectively, for the slope and deflection under uniformly distributed loads (UDL) using the thin beam theory [Popov (1990)]; the same beam configurations are solved by applying the nonlinear electrostatic force field. The thin beam governing equation [Timoshenko and Goodier (1970); Popov (1990)] is,

$$EI\frac{d^4w(x)}{dx^4} = q(x) \text{ (by Timoshenko thin beam theory)} \tag{49}$$

where, $q(x)$ is an applied load, EI is Flexural rigidity, and w is the beam deflection. Fixed-fixed beam under UDL is solved with the boundary conditions,

$$w(x=0)=0,\ w(x=L)=0,\ \frac{dw(x=0)}{dx}=0 \text{ and } \frac{dw(x=L)}{dx}=0 \tag{50}$$

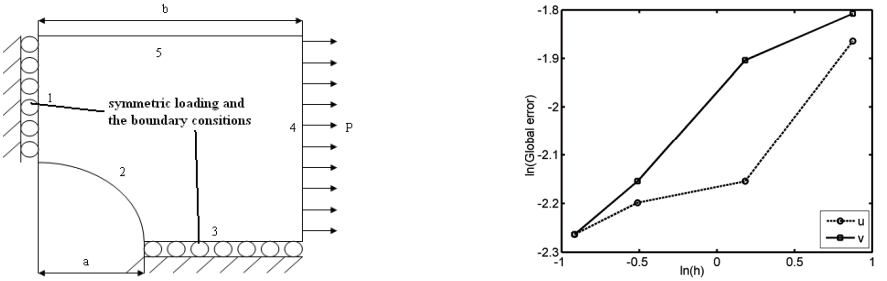

a **b**

Figure 18: Semi-infinite plate with a central load a) schematic of the computational domain, b) u and v displacement convergence plots by uniform field nodes.

The beam parameters are $q=-3.0$ N, $E=3\times10^7$ Pa, $\nu=0.3$, $length(L)=20$ m, $thickness(t)=0.1$ m and $width(D)=1.0$ m. The deflection and slope analytical solutions are given as,

$$w(x)=\frac{q\,x^2\,(L-x)^2}{24\,EI} \text{ and } \frac{dw(x)}{dx}=\frac{q}{EI}\left[\frac{x\,L^2}{12}-\frac{L\,x^2}{4}+\frac{x^3}{6}\right] \tag{51}$$

The problem is solved by 41 uniform and random, field and virtual nodes, respectively; corresponding solutions are plotted in Figs. 21a and 21b, respectively. The nonlinear electrostatic force field is applied on the fixed-fixed beam as given,

$$q(x)=\frac{\varepsilon_0\,\tilde{v}^2\,\tilde{w}}{2\,g^2}\left[1+\,0.65\,\frac{g}{\tilde{w}}\right] \tag{52}$$

Where, ε_0, $\tilde{v}$, $\tilde{w}$ are the vacuum permittivity $\left(8.8541878176\times10^{-12}\text{ F / m}\right)$, applied voltage and the beam width, respectively, and $g=g_0-w(x)$ where, g_0 is an initial gap between the beam and bottom fixed plate. The beam parameters are $\tilde{v}=15.05$ volt, $E=169$ GPa, $\nu=0.3$, $L=80\,\mu$m, $t=0.5\,\mu$m and $\tilde{w}=10\,\mu$m. As the beam starts to deflect due to applied electrostatic force field given by Eq. (52), the load becomes nonlinear. Thus, it becomes an implicit problem which needs to be solved by inner iterations with a relaxation technique. For the given beam

parameters, beam deflection is plotted in Fig. 22a, and Fig. 22b show the peak deflection convergence during the inner iterations. It can be seen from Fig. 22a that the field node deflection values are smoothly computed, which demonstrate that the RDQ method can effectively handle the nonlinear deformation problems. In order to compare the results, the inner iterations are carried out by fixed point and Newton methods and both gave equal results.

A cantilever beam (Fig. 20b) under the UDL is solved with boundary conditions as,

$$w(x=0)=0,\ \frac{dw(x=0)}{dx}=0 \text{ and } \frac{d^2w(x=L)}{dx^2}=0,\ \frac{d^3w(x=L)}{dx^3}=0 \tag{53}$$

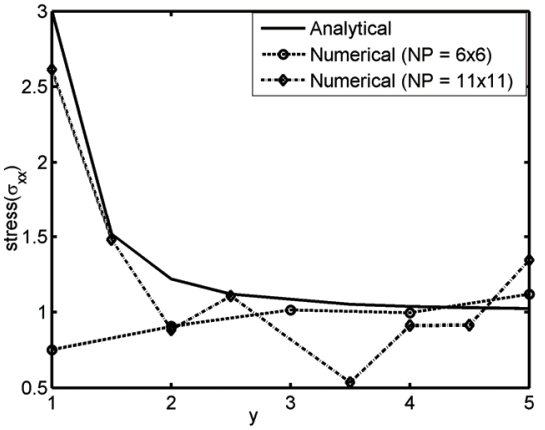

Figure 19: Numerical and analytical stress, σ_{xx}, comparison along the boundary 1. As the field nodes are increased, the maximum numerical σ_{xx} value approaches its analytical value.

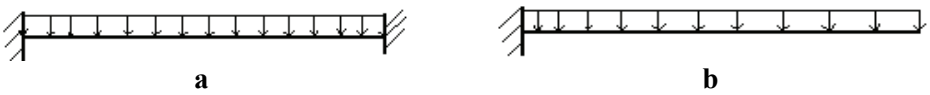

Figure 20: a) Schematic of a fixed-fixed beam under the UDL, b) Schematic of a cantilever beam under the UDL.

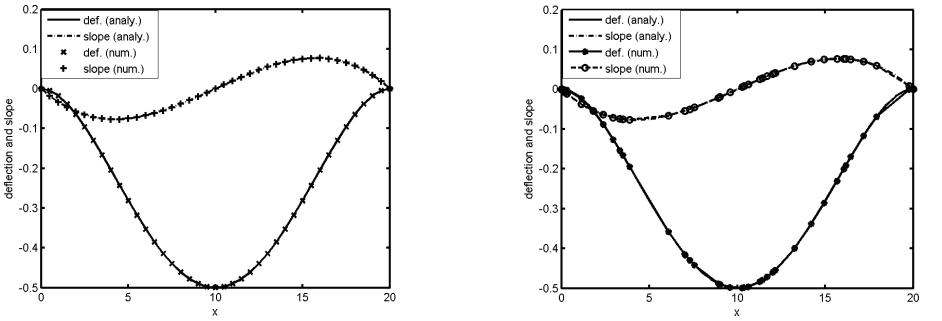

Figure 21: Numerical and analytical deflection and slope values comparison for a fixed-fixed beam under the UDL by a) uniform, b) random, field nodes.

All the beam parameters are same as fixed-fixed beam with analytical solutions as,

$$w(x) = \frac{q}{24\,EI}\left[x^4 - 4x^3L + 6x^2L^2\right] \text{ and } \frac{dw(x)}{dx} = \frac{q}{EI}\left[\frac{x^3}{6} - \frac{L\,x^2}{2} + \frac{x^2L}{2}\right] \tag{54}$$

This problem is solved by 41 uniform and random, field and virtual nodes, respectively; the corresponding numerical solutions are given in Figs. 23a and 23b. The nonlinear electrostatic force field is applied on the cantilever beam as given in Eq. (52). The beam parameters used are $\tilde{v} = 2.64453$ volt, $E = 169$ GPa, $\nu = 0.3$, $L = 80\,\mu$m, $t = 0.5\,\mu$m and $\tilde{w} = 10\,\mu$m.

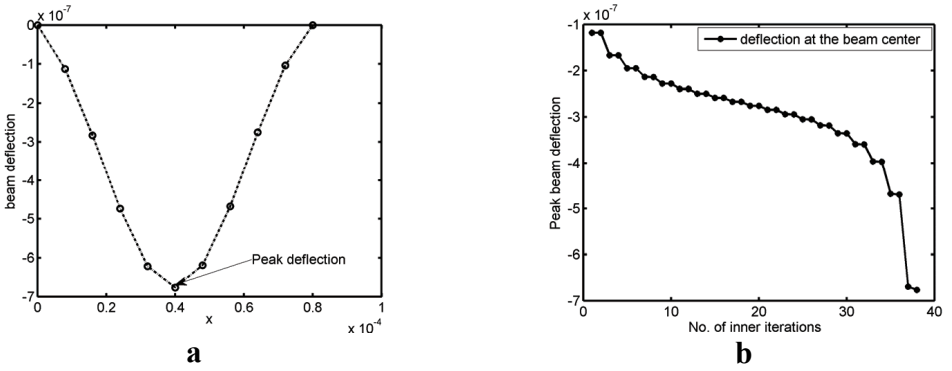

Figure 22: Fixed-fixed beam under the influence of nonlinear electrostatic load a) beam deflection due to $\tilde{v} = 15.05$ volt, b) peak deflection convergence with the inner iterations.

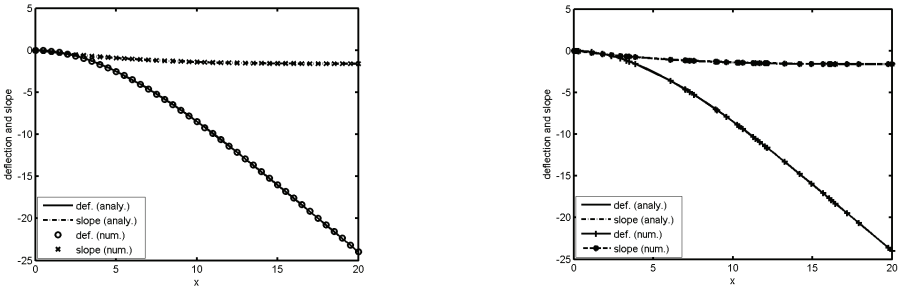

Figure 23: Numerical and analytical deflection and slope values comparison for a cantilever beam under the UDL by a) uniform, b) random, field nodes.

For Newton iteration technique, there should be only one discretization equation per node but if Eq. (53) is observed, it is seen that two boundary conditions are applied at each of the leftmost and rightmost domain nodes. Hence, this difficulty is overcome by transferring one of the boundary conditions at the leftmost and rightmost nodes to their neighbouring nodes as given,

$$\left(\frac{dw}{dx}\right)_1 = \frac{(w_2 - w_1)}{(x_2 - x_1)} = 0, \text{ as } w_1 = 0, \text{ so } w_2 = 0$$

and

$$w_{,xxx}|_N = \frac{w_{,xx}|_N - w_{,xx}|_{N-1}}{x_N - x_{N-1}} = 0, \text{ as } w_{,xx}|_N = 0, \quad w_{,xx}|_{N-1} = 0 \tag{55}$$

where, w_1, w_2, and x_1, x_2 are the deflections and co-ordinates at the node 1 and 2, respectively, and N is the total nodes. The modified boundary conditions are as,

$$w_1 = 0,\ w_2 = 0 \text{ and } \left(\frac{d^2w}{dx^2}\right)_N = 0, \ \left(\frac{d^2w}{dx^2}\right)_{N-1} = 0 \tag{56}$$

Using Eq. (56) with Eqs. (49) and (52), Newton method is employed at the virtual nodes with the residual, $R = KU - F$, as a function. The virtual node deflection values at n^{th} iteration, where, $n > 1$, are computed by the deflections values at the 0^{th} and 1^{st} iteration as given,

$$J\left[\frac{\partial R(w^1_{vir})}{\partial w}\right] \left[w^2_{vir} - w^1_{vir}\right] = -R\left(w^1_{vir}\right) \text{ applied at } j^{th} \text{ virtual node} \tag{57}$$

$$J\left[\frac{\partial R(w^1_{vir})}{\partial w}\right]_j = \frac{k_j U^1 - k_j U^0}{w^1_j - w^0_j} - \left.\frac{\partial F(w^1)}{\partial w}\right|_j, \quad \left.\frac{\partial F(w^1)}{\partial w}\right|_j = \frac{F(w^1_j) - F(w^0_j)}{w^1_j - w^0_j},$$

and

$$R(w^1)_j = K_j U^1 - F(w_j^1) \tag{58}$$

where $J\left[\frac{\partial R(w_{vir}^1)}{\partial w}\right]_j$ is Jacobean matrix computed at j^{th} virtual node by the residual function R. Eqs. (57) and (58) are solved together iteratively till the peak deflection field node value converges. For the given beam parameters, the beam deflection is computed by Newton method as explained and plotted in Fig. 24a, and Fig. 24b shows the peak deflection convergence during the inner iterations.

All the results obtained by solving the elasticity problems shows that the RDQ method can effectively handle different field variable distribution orders in the engineering problems. The results obtained by applying the nonlinear electrostatic force field on the fixed-fixed and cantilever beam analysis shows that the RDQ method can be successfully applied to solve the nonlinear differential equations in the mechanics.

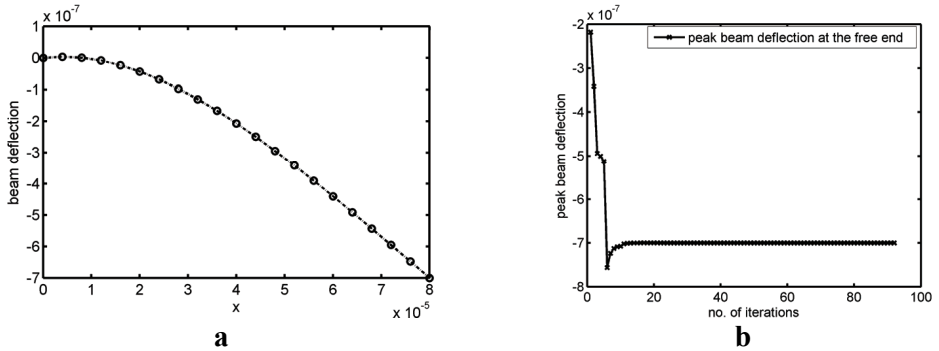

Figure 24: For a cantilever beam under the influence of nonlinear electrostatic loading a) beam deflection plot, b) peak beam deflection convergence during the inner iterations.

7 Conclusions

In this paper, a novel strong-form meshless method called the RDQ method is developed. For the RDQ method, the superconvergence condition is developed and the RDQ method convergence analysis is carried out using it. It is observed that if the number of field nodes are computed by the superconvergence condition, the function and its approximate derivatives converge at the rate $O(h^{p+\alpha})$, where

$\alpha \geq 1$ for the function approximation and $\alpha \approx 0.7$ to 1 for its derivative approximation. The convergence analysis also shows that if the complete and consistent order monomials are included in the function approximation, the function and its derivatives are exactly reproduced. The RDQ method is successfully demonstrated to solve the fixed-fixed and cantilever beams loaded by the nonlinear electrostatic force field. It is observed from all the convergence plots and values that the RDQ method effectively handles the randomly distributed field nodes and sometimes performs even better than the uniform field nodes. It is also seen that the weighted derivatives approach effectively computes the 1^{st}- and 2^{nd}-order function derivatives.

Acknowledgement: The authors gratefully acknowledge the financial support from Sun Microsystems Inc. through a collaborative research with Nanyang Technological University, Singapore under the project number: M48050114.

References

Aluru, N. R. (1999): A reproducing kernel particle method for meshless analysis of microelectromechanical systems. *Comput Mech,* vol. 23, pp. 324-338.

Aluru, N. R. (2000): A point collocation method based on reproducing kernel approximations. *Int J Numer Meth Eng*, vol. 47, pp. 1083-1121.

Aluru, N. R.; Li, G. (2001): Finite cloud method: a true meshless technique based on a fixed reproducing kernel approximation. *Int J Numer Meth Eng*, vol. 50, pp. 2373-2410.

Arefmanesh, A.; Najafi, M.; Abdi, H. (2008): Meshless Local Petrov-Galerkin Method with Unity Test Function for Non-Isothermal Fluid Flow. *CMES: Computer Modeling in Engineering and Sciences*, vol. 25, No. 1, pp. 9-22.

Atluri, S. N. (2004): The meshless method (MLPG) for domain & BIE discretizations. Tech Science Press, Forsyth.

Atluri, S. N. (2005): Methods of computer modeling in engineering & the sciences. Tech Science Press, Forsyth.

Atluri, S. N.; Cho, J. Y.; Kim, H. G. (1999): Analysis of thin beams, using meshless local Petrov-Galerkin method, with generalized moving least square interpolations. *Comput Mech,* vol. 24, pp. 334-347.

Atluri, S. N.; Han, Z. D.; Rajendran, A. M. (2004): A new implementation of the meshless finite volume method, through the MLPG "mixed" approach. *CMES: Computer Modeling in Engineering and Sciences*, vol. 6, No. 6, pp. 491-513.

Atluri, S. N.; Kim, H. G.; Cho, J. Y. (1999): A critical assessment of the truly

meshless Local Petrov-Galerkin (MLPG), and local Boundary Integral Equation (LBIE) methods. *Comput Mech,* vol. 24, pp. 348-372.

Atluri, S. N.; Liu, H. T.; Han, Z. D. (2006a): Meshless Local Petrov-Galerkin (MLPG) mixed collocation method for elasticity problems. *CMES: Computer Modeling in Engineering and Sciences*, vol. 14, No. 3, pp. 141-152.

Atluri, S. N.; Liu, H. T.; Han, Z. D. (2006b): Meshless Local Petrov-Galerkin (MLPG) mixed finite difference method for solid mechanics. *CMES: Computer Modeling in Engineering and Sciences*, vol. 15, No. 1, pp. 1-16.

Atluri, S. N.; Shen, S. (2002): The meshless local Petrov-Galerkin method. Tech Science Press, Encino.

Atluri, S. N.; Sladek, J.; Sladek, V.; Zhu, T. (2000): The local boundary integral equation (LBIE) and its meshless implementation for linear elasticity. *Comput Mech,* vol. 25, pp. 180-189.

Atluri, S. N.; Zhu, T. (1998): A new Meshless Local Petrov-Galerkin (MLPG) approach in computational mechanics. *Comput Mech,* vol. 22, pp. 117-127.

Bellman, R. E.; Kashef, B. G.; Casti, J. (1972): Differential quadrature: a technique for the rapid solution of nonlinear partial differential equations. *J Comput Phys,* vol. 10, pp. 40–52.

Belytschko, T.; Gu, L.; Lu, Y. Y. (1994): Fracture and crack growth by element free Galerkin method. *Model Simulat Mater Sci Eng,* vol. 2, pp. 519-534.

Belytschko, T.; Lu, Y. Y.; Gu, L. (1994): Element-Free Galerkin Methods. *Int J Numer Meth Eng*, vol. 37, pp. 229-256.

Bonet, J.; Lok, T. -S. L. (1998): Variational and momentum preservation aspects of Smooth Particle Hydrodynamic formulations. *Comput Meth Appl Mech Eng,* vol. 180, pp. 97-115.

Braun, J.; Sambridge, M. (1995): A numerical method for solving partial differential equations on highly irregular evolving grids. *Nature*, vol. 376, pp. 655-660.

Cai, Y. C.; Zhu, H. H. (2008): A Local Meshless Shepard and Least Square Interpolation Method Based on Local Weak Form. *CMES: Computer Modeling in Engineering and Sciences*, vol. 34, No. 2, pp. 179-204.

Chen, S. S.; Liu, Y. H.; Cen, Z. Z. (2008): A Combined Approach of the MLPG Method and Nonlinear Programming for Lower-Bound Limit Analysis. *CMES: Computer Modeling in Engineering and Sciences*, vol. 28, No. 1, pp. 39-55.

Christoph, U. (1997): Numerical computation: methods, software, and analysis. Springer-Verlag, Germany.

Dang, T. D.; Sankar, B. V. (2008): Meshless Local Petrov-Galerkin Micromechan-

ical Analysis of Periodic Composites Including Shear Loadings. *CMES: Computer Modeling in Engineering and Sciences*, vol. 26, No. 3, pp. 169-187.

Ding, H.; Shu, C.; Yeo, K. S.; Xu, D. (2006): Numerical computation of three-dimensional incompressible viscous flows in the primitive variable form by local multiquadric differential quadrature method. *Comput Meth Appl Mech Eng,* vol. 195, pp. 516-533.

Gilhooley, D. F.; Xiao, J. R.; Batra, R. C.; McCarthy, M. A.; Gillespie, J. W. (2008): Two-dimensional stress analysis of functionally graded solids using the MLPG method with radial basis functions. *Comput Mater Sci*, vol. 41, pp. 467-481.

Gingold, R. A.; Monaghan, J. J. (1977): Smoothed particle hydrodynamics: theory and application to non-spherical stars. *Mon Not Roy Astron Soc Lett*, vol. 181, pp. 375-389.

Han, Z. D.; Liu, H. T.; Rajendran, A. M.; Atluri, S. N. (2006): The applications of Meshless Local Petrov-Galerkin (MLPG) approaches in high-speed impact, penetration and perforation problems. *CMES: Computer Modeling in Engineering and Sciences*, vol. 14, No. 2, pp. 119-128.

Han, Z. D.; Rajendran, A. M.; Atluri, S. N. (2005): Meshless Local Petrov-Galerkin (MLPG) approaches for solving nonlinear problems with large deformations and rotations. *CMES: Computer Modeling in Engineering and Sciences*, vol. 10, No. 1, pp. 1-12.

Haq, S.; Siraj, U. I.; Ali, A. (2008): A Numerical Meshfree Technique for the Solution of the MEW Equation. *CMES: Computer Modeling in Engineering and Sciences*, vol. 38, No. 1, pp. 1-23.

Haq, S.; Siraj, U. I.; Uddin, M. (2009): Numerical Solution of Nonlinear Schrodinger Equations by Collocation Method Using Radial Basis Functions. *CMES: Computer Modeling in Engineering and Sciences*, vol. 44, No. 2, pp. 115-135.

Idelsohn, S. R.; Onate, E.; Calvo, N.; Pin, F. D. (2003): The meshless finite element method. *Int J Numer Meth Eng*, vol. 58, pp. 893-912.

Jarak, T.; Soric, J.; Hoster, J. (2007): Analysis of shell deformation responses by the meshless local Petrov-Galerkin (MLPG) approach. *CMES: Computer Modeling in Engineering and Sciences*, vol. 18, No. 3, pp. 235-246.

Jin, X.; Li, G.; Aluru, N. R. (2001): On the Equivalence Between Least-Squares and Kernel Approximations in Meshless Methods. *CMES: Computer Modeling in Engineering and Sciences*, vol. 2, No. 4, pp. 447-462.

Jin, X.; Li, G.; Aluru, N. R. (2004): Positivity conditions in meshless collocation methods. *Comput Meth Appl Mech Eng,* vol. 193, pp. 1171-1202.

Jin, X.; Li, G.; Aluru, N. R. (2005): New approximations and collocation schemes in the finite cloud method. *Comput Struct*, vol. 83, pp. 1366-1385.

Kosec, G.; Šarler, B. (2008): Local RBF Collocation Method for Darcy Flow. *CMES: Computer Modeling in Engineering and Sciences,* vol. 25, No. 3, pp. 197-207.

Le, P.; Mai-Duy, N.; Tran-Cong, T.; Baker, G. (2008): A Meshless Modeling of Dynamic Strain Localization in Quasi-Brittle Materials Using Radial Basis Function Networks. *CMES: Computer Modeling in Engineering and Sciences,* vol. 25, No. 1, pp. 43-66.

Li, S.; Atluri, S. N. (2008): Topology-optimization of Structures Based on the MLPG Mixed Collocation Method. *CMES: Computer Modeling in Engineering and Sciences,* vol. 26, No. 1, pp. 61-74.

Li, H.; Cheng, J. Q.; Ng, T. Y.; Chen, J.; Lam, K. Y. (2004): A meshless Hermite-cloud method for nonlinear fluid-structure analysis of near-bed submarine pipelines under current. *Eng Struct,* vol.26, pp. 531-542.

Li, L.; Liu, S.; Wang, H. (2008): Meshless Analysis of Ductile Failure. *CMES: Computer Modeling in Engineering and Sciences,* vol. 36, No. 2, pp. 173-191.

Li, H.; Ng, T. Y.; Cheng, J. Q.; Lam, K. Y. (2003): Hermite–Cloud: a novel true meshless method. *Comput Mech*, vol. 33, pp. 30-41.

Li, G.; Paulino, G. H.; Aluru, N. R. (2003): Coupling of the mesh-free finite cloud method with the boundary element method: a collocation approach. *Comput Meth Appl Mech Eng,* vol. 192, pp. 2355-2375.

Li, H.; Wang, Q. X.; Lam, K. Y. (2004): Development of a novel meshless Local Criging (LoKriging) method for structural dynamics analysis. *Comput Meth Appl Mech Eng,* vol. 193, pp. 2599-2619.

Li, H.; Yew, Y. K.; Ng, T. Y.; Lam, K. Y. (2005): Meshless steady-state analysis of chemo-electro-mechanical coupling behaviour of pH-sensitive hydrogel in buffered solution. *J Electroanal Chem,* vol. 580, pp. 161-172.

Liew, K. M.; Huang, Y. Q.; Reddy, J. N. (2003): Moving least squares differential quadrature method and its application to the analysis of shear deformable plates. *Int J Numer Meth Eng*, vol. 56, pp. 2331-2351.

Liew, K. M.; Huang, Y. Q.; Reddy, J. N. (2004): Analysis of general shaped thin plates by the moving least-squares differential quadrature method. *Finite Elem Anal Des*, vol. 40, pp. 1453-1474.

Liew, K. M.; Zhang, J. Z.; Ng, T. Y.; Meguid, S. A. (2003): Three-dimensional modelling of elastic bonding in composite laminates using layerwise differential quadrature. *Int J Solids Struct*, vol. 40, pp. 1745-1764.

Liu, C. S. (2007a): A Meshless Regularized Integral Equation Method for Laplace Equation in Arbitrary Interior or Exterior Plane Domains. *CMES: Computer Modeling in Engineering and Sciences*, Vol. 19, No. 1, pp. 99-109.

Liu, C. S. (2007b): A MRIEM for Solving the Laplace Equation in the Doubly-Connected Domain. *CMES: Computer Modeling in Engineering and Sciences*, Vol. 19, No. 2, pp. 145-161.

Liu, Y. H.; Chen, S. S.; Li, J.; Cen, Z. Z. (2008): A Meshless Local Natural Neighbour Interpolation Method Applied to Structural Dynamic Analysis. *CMES: Computer Modeling in Engineering and Sciences*, Vol. 31, No. 3, pp. 145-156.

Liu, W. K.; Chen, Y.; Uras, R. A.; Chang, C. T. (1996): Generalized multiple scale reproducing kernel particle method. *Comput Meth Appl Mech Eng,* vol. 139, pp. 91-157.

Liu, G. R.; Gu, Y. T. (2001): A point interpolation method for two-dimensional solids. *Int J Numer Meth Eng,* vol. 50, pp. 937-951.

Liu, W. K.; Jun, S. (1998): Multiple Scale Reproducing Kernel Particle Methods for Large Deformation Problems. *Int J Numer Meth Eng,* vol. 41, pp. 1339-1362.

Liu, W. K.; Jun, S.; Zhang, Y. F. (1995): Reproducing Kernel Particle Methods. *Int J Numer Meth Fluid,* vol. 20, pp. 1081-1106.

Liu, G. R.; Zhang, J.; Lam, K. Y.; Li, H.; Xu, G.; Zhong, Z. H.; Li, G. Y.; Han, X. (2008): A gradient smoothing method (GSM) with directional correction for solid mechanics problems. *Comput Mech,* vol. 41, pp. 457-472.

Liu, G. R.; Zhang, J.; Li, H.; Lam, K. Y.; Bernard, Kee, B. T. (2006): Radial point interpolation based finite difference method for mechanics problems. *Int J Numer Meth Eng,* vol. 68, pp. 728-754.

Long, S. Y.; Liu, K. Y.; Li, G. Y. (2008): An Analysis for the Elasto-Plastic Fracture Problem by the Meshless Local Petrov-Galerkin Method. *CMES: Computer Modeling in Engineering and Sciences*, vol. 28, No. 3, pp. 203-216.

Lu, Y. Y.; Belytschko, T.; Gu, L. (1994): A new implementation of the element free Galerkin method. *Comput Meth Appl Mech Eng*, vol. 113, pp. 397-414.

Lucy, L. B. (1977): A numerical approach to testing the fission hypothesis. *Astronom J*, vol. 8, pp. 1013-1024.

Ma, Q. W. (2007): Numerical generation of freak waves using MLPG_R and QALE-FEM methods. *CMES: Computer Modeling in Engineering and Sciences*, vol. 18, No. 3, pp. 223-234.

Ma, Q. W. (2008): A New Meshless Interpolation Scheme for MLPG_RMethod. *CMES: Computer Modeling in Engineering and Sciences*, vol. 23, No. 2, pp. 75-89.

Ma, Q. W.; Yan, S. (2006): Quasi ALE finite element method for nonlinear water waves. *J Comput Phys*, vol. 212, pp. 52-72.

Ma, Q. W.; Zhou, J. T. (2009): MLPG_R method for numerical simulation of 2D breaking waves. *CMES: Computer Modeling in Engineering and Sciences*, vol. 43, No. 3, pp. 277-303.

Mai-Cao, L.; Tran-Cong, T. (2005): A meshless IRBFN-based method for transient problems. *CMES: Computer Modeling in Engineering and Sciences*, vol. 7, No. 2, pp. 149-171.

Mai-Cao, L.; Tran-Cong, T. (2008): A Meshless Approach to Capturing Moving Interfaces in Passive Transport Problems. *CMES: Computer Modeling in Engineering and Sciences*, vol. 31, No. 3, pp. 157-188.

Melenk, J. M.; Babuska, I. (1996): The partition of unity finite element method: basic theory and applications. *Comput Meth Appl Mech Eng*, vol. 139, pp. 289-314.

Mukherjee, Y. X.; Mukherjee, S. (1997): On boundary conditions in the element-free Galerkin method. *Comput Mech,* vol. 19, pp. 264-270.

Mulay, S. S.; Li, H. (2009): Analysis of Microelectromechanical Systems Using the Meshless Random Differential Quadrature Method. *Advanced Materials Research*, vol. 74, pp. 29-32.

Nayroles, B.; Touzot, G.; Villon, P. (1992): Generalizing the finite element method: Diffuse approximation and diffuse elements. *Comput Mech,* vol. 10, pp. 307-318.

Naadimuthu, G.; Bellman, R.; Wang, K. M. (1984): Differential quadrature and partial differential equations: some numerical results. *J Math Anal Appl*, vol. 98, pp. 220-235.

Onate, E.; Idelsohn, E. O.; Zienkiewicz, O. C.; Taylor, R. L. (1996): A finite point method in computational mechanics. Applications to convective transport and fluid flow. *Int J Numer Meth Eng*, vol. 39, pp. 3839-3866.

Onate, E.; Idelsohn, E. O.; Zienkiewicz, O. C.; Taylor, R. L.; Sacco, C. (1996): A stabilized finite point method for analysis of fluid mechanics problems. *Comput Meth Appl Mech Eng,* vol. 139, pp. 315-346.

Pini, G.; Mazzia, A.; Sartoretto, F. (2008): Accurate MLPG Solution of 3D Potential Problems. *CMES: Computer Modeling in Engineering and Sciences*, vol. 36, No. 1, pp. 43-63.

Popov, E. P. (1990): Engineering Mechanics of Solids. Prentice Hall, New Jersey.

Quan, J. R.; Chang, C. T. (1989a): New insights in solving distributed system equations by the quadrature method– I. Analysis. *Comput Chem Eng,* vol. 13, pp. 779-788.

Quan, J. R.; Chang, C. T. (1989b): New insights in solving distributed system equations by the quadrature method–II. Numerical experiments. *Comput Chem Eng,* vol. 13, pp. 1017-1024.

Reutskiy, S. Y. (2008): Meshless Method for Nonlinear, Singular and Generalized Sturm-Liouville Problems. *CMES: Computer Modeling in Engineering and Sciences*, vol. 34, No. 3, pp. 227-252.

Sarra, S. A. (2006): Chebyshev Interpolation: An Interactive Tour. *Journal of Online Mathematics and Its Applications*, vol. 6, pp. 1-13.

Shan, Y. Y.; Shu, C.; Lu, Z. L. (2008): Application of Local MQ-DQ Method to Solve 3D Incompressible Viscous Flows with Curved Boundary. *CMES: Computer Modeling in Engineering and Sciences*, vol. 25, No. 2, pp. 99-113.

Shaw, A.; Banerjee, B.; Roy, D. (2008): A NURBS-based parametric method bridging mesh-free and finite element formulations. *CMES: Computer Modeling in Engineering and Sciences*, vol. 26, No. 1, pp. 31-57.

Shaw, A.; Roy, D. (2007): A novel form of reproducing kernel interpolation method with applications to nonlinear mechanics. *CMES: Computer Modeling in Engineering and Sciences*, vol. 19, No. 1, pp. 69-98.

Shu, C. (2000): Differential Quadrature and its application in Engineering. Springer-Verlag, London.

Shu, C.; Khoo, B. C.; Yeo, K. S. (1994): Numerical solutions of incompressible Navier-Stokes equations by generalized differential quadrature. *Finite Elem Anal Des*, vol. 18, pp. 83-97.

Sladek, J.; Sladek, V.; Solek, P.; Atluri, S. N. (2008): Modeling of Intelligent Material Systems by the MLPG. *CMES: Computer Modeling in Engineering and Sciences*, vol. 34, No. 3, pp. 273-300.

Sladek, J.; Sladek, V.; Solek, P.; Wen, P. H. (2008): Thermal Bending of Reissner-Mindlin Plates by the MLPG. *CMES: Computer Modeling in Engineering and Sciences*, vol. 28, No. 1, pp. 57-76.

Sladek, J.; Sladek, V.; Tan, C. L.; Atluri, S. N. (2008): Analysis of Transient Heat Conduction in 3D Anisotropic Functionally Graded Solids, by the MLPG Method. *CMES: Computer Modeling in Engineering and Sciences*, vol. 32, No. 3, pp. 161-174.

Sladek, J.; Sladek, V.; Zhang, Ch.; Solek, P. (2007): Application of the MLPG to thermo-piezoelectricity. *CMES: Computer Modeling in Engineering and Sciences*, vol. 22, No. 3, pp. 217-233.

Sladek, J.; Sladek, V.; Zhang, Ch.; Solek, P.; Starek, L. (2007): Fracture analyses in continuously nonhomogeneous piezoelectric solids by the MLPG. *CMES:*

Computer Modeling in Engineering and Sciences, vol. 19, No. 3, pp. 247-262.

Sukumar, N.; Moran, B.; Belytschko, T. (1998): The natural element method in solid mechanics. *Int J Numer Meth Eng,* vol. 43, pp. 839-887.

Sukumar, N.; Moran, B.; Semenov, A. Y.; Belicov, V. V. (2001): Natural neighbour Galerkin methods. *Int J Numer Meth Eng*, vol. 50, pp. 1-27.

Timoshenko, S. P.; Goodier, J. N. (1970): Theory of Elasticity, third ed. McGraw-Hill, New York.

Wong, S.; Shie, Y. (2008): Large Deformation Analysis with Galerkin based Smoothed Particle Hydrodynamics. *CMES: Computer Modeling in Engineering and Sciences*, vol. 36, No. 2, pp. 97-117.

Wu, C.; Chiu, K.; Wang, Y. (2008): A Differential Reproducing Kernel Particle Method for the Analysis of Multilayered Elastic and Piezoelectric Plates. *CMES: Computer Modeling in Engineering and Sciences*, vol. 27, No. 3, pp. 163-186.

XueHong, W. U.; Shen, S.; Tao, W. (2007): Meshless local Petrov-Galerkin collocation method for two-dimensional heat conduction problems. *CMES: Computer Modeling in Engineering and Sciences*, vol. 22, No. 1, pp. 65-76.

Young, D. L.; Chen K. H.; Lee, C. W. (2005): Novel meshless method for solving the potential problems with arbitrary domain. *J Comput Phys*, vol. 209, pp. 290-321.

Young, D. L.; Chen K. H.; Lee, C. W. (2006): Singular meshless method using double layer potentials for exterior acoustics. *J Acoust Soc Am*, vol. 119, No. 1, pp. 96-107.

Zheng, J.; Long, S.; Xiong, Y.; Li, G. (2009): A Finite Volume Meshless Local Petrov-Galerkin Method for Topology Optimization Design of the Continuum Structures. *CMES: Computer Modeling in Engineering and Sciences*, vol. 42, No. 1, pp. 19-34.

Zhilun, X. (1992): Applied Elasticity (Eng.). New Age International (p) Ltd, India.

Zhu, T.; Zhang, J. D.; Atluri, S. N. (1998): A local boundary integral equation (LBIE) method in computational mechanics and a meshless discretization approach. *Comput Mech,* vol. 21, pp. 223-235.

Zong, Z.; Lam, K. Y. (2002): A localized differential quadrature (LDQ) method and its application to 2D wave equation. *Comput Mech,* vol. 29, pp. 382-391.